2016

Hybrid straintronics-spintronics: Energy-efficient non-volatile devices for Boolean and non-Boolean computation

Ayan K. Biswas
Virginia Commonwealth University, biswasak@vcu.edu

HYBRID STRAINTRONICS-SPINTRONICS: ENERGY-EFFICIENT NON-

VOLATILE DEVICES FOR BOOLEAN AND NON-BOOLEAN COMPUTATION

A Dissertation submitted in partial fulfillment of the requirements for the degree of Doctor of Philosophy in Engineering at Virginia Commonwealth University.

by

AYAN KUMAR BISWAS
Bachelor of Science in Electrical and Electronic Engineering, Bangladesh University of Engineering and Technology, 2011

Doctoral committee chairperson: Prof. Supriyo Bandyopadhyay
Commonwealth Professor, Department of Electrical and Computer Engineering

Virginia Commonwealth University
Richmond, Virginia
May 2016

Acknowledgements

I would like to express my heartiest gratitude to my PhD supervisor Prof. Supriyo Bandyopadhyay without whose continuous support I doubt that I would be writing this thesis. Spending all these years under his supervision, I have learnt a lot about conducting a fruitful research. His profound knowledge on Spintronics and nanomagnetism has extremely helped me to understand many complex research topics. I feel extremely privileged to get an opportunity to work under such a scholar like him. I am also thankful to him not only to supervise me in my research projects but also in finding the right directions while evolving as a researcher. Without his invaluable help, precious comments, and careful guidance this journey of pursuing graduate study would not be so successful today. I would also like to express my gratitude to Prof. Jayasimha Atulasimha for being my co-advisor in all my research projects and for playing a highly significant role in conducting both academic and professional development.

I am thankful to my peers who have been my companions during this endeavor and with whom I have worked and shared the ideas, namely, Md. Iftekhar Hossain, Dr. Noel D'Souza, Vimal Sampath, Md Mamun Al-Rashid, Dhritiman Bhattacharya, Pallabi Sutradhar, Md. Ahsanul Abdeed, Justine Drobitch and especially Hasnain Ahmad without whose help the experiment would not have been possible. I would also like to show my gratitude to Prof. Ümit Özgür, Prof. Gary M. Atkinson and Prof. Shiv N. Khanna for being a part of my PhD committee and for their significant comments on my research projects. I

also offer my thanks to the staffs of the Electrical and Computer Engineering department, the Wright Virginia Microelectronics Center, and Nanomaterials Characterization Center. Final professional acknowledgements go to the National Science Foundation (NSF) under the NEB2020 grant ECCS-1124714 SHF Grant CCF-1216614 and NSF CAREER grant CCF-1253370 as well as the Semiconductor Research Company (SRC) under NRI task 2203.001 for funding this research.

I would finally want to thank my parents, Noni Gopal Biswas and Sneha Lata Biswas, my brothers Dipon Biswas and Preetom Biswas, my wife Chaiti Rani Kundu for their love, support and motivation towards achieving the success in both academic and personal lives.

Table of contents

List of Figures

List of Tables

Abstract

HYBRID STRAINTRONICS-SPINTRONICS: ENERGY-EFFICIENT NON-VOLATILE DEVICES FOR BOOLEAN AND NON-BOOLEAN COMPUTATION

A Dissertation submitted in partial fulfillment of the requirements for the degree of Doctor of Philosophy in Engineering at Virginia Commonwealth University.

by

AYAN KUMAR BISWAS
Bachelor of Science in Electrical and Electronic Engineering, Bangladesh University of Engineering and Technology, 2011

Doctoral committee chairperson: Prof. Supriyo Bandyopadhyay
Commonwealth Professor, Department of Electrical and Computer Engineering

Research in future-generation computing is focused on reducing energy dissipation while maintaining the switching speed in a binary operation to continue the current trend of increasing transistor-density on a chip according to Moore's law. Unlike charge-based CMOS technology, spin-based nanomagnetic technology, predicated on using single domain shape-anisotropic nanomagnets with bistable magnetization states as a binary switch, has the potential to achieve ultralow energy dissipation due to the fact that no charge motion is directly involved in switching. However, switching of magnetization has not been any less dissipative than switching transistors because most magnet switching schemes involve generating a current to produce a magnetic field, or spin transfer torque, or domain wall motion, to switch magnetization. Current-induced switching invariably dissipates an exorbitant amount of energy in the switching circuit that nullifies any energy advantage that a magnet may have over a transistor. Magnetoelastic switching (switching the magnetization of a magnetostrictive magnet with voltage generated stress) is an unusual switching paradigm where the dissipation turns out to be merely few hundred kT per switching event − several orders of magnitude less than that encountered in current-based switching. A fundamental obstacle, though, is to deterministically switch the magnetization of a nanomagnet between two stable states that are mutually anti-parallel with stress alone. In this work, I have investigated ways to mitigate this problem.

One popular approach to flip the magnetizations of a nanomagnet is to pass a spin polarized current through it that transfers spin angular moment from the current to the electrons in the magnet, thereby switching their spins and ultimately the magnet's

magnetization. This approach – known as spin transfer torque (STT) – is very dissipative because of the enormous current densities needed to switch magnets, We, therefore, devised a mixed mode technique to switch magnetization with a combination of STT and stress in order to capitalize on the energy-efficiency of stress-based switching and determinism of STT based switching. This approach reduces the total energy dissipation by roughly one order of magnitude compared to pure STT-based switching. We then extended this idea to find a way to deterministically flip magnetization with stress alone, in the hope that it will further reduce energy disssipation. Sequentially applying stresses along two skewed axes, a complete 180° switching of magnetization can be achieved. These results have been verified with stochastic Landau-Lifshitz-Gilbert simulation in the presence of thermal noise. Elliptical cobalt nanomagnets of 200-300 nm lateral dimensions have been fabricated on a PMN-PT substrate. Their magnetizations have two stable states along the major axes. The nanomagnets are first magnetized in one direction along the major axis with an external magnetic field. Subsequent application of stress along two directions (neither coinciding with the major or minor axis), generated by electric fields imposed across the piezoelectric PZT substrate in those directions with two pairs of electrodes, indeed rotated the nanomagnets' magnetizations through $\sim 180^0$ as verified with magnetic force microscopy. Thus, we were able to switch the magnetization from one stable state to another with stress alone and implement a "straintronic" nanomagnetic switch. This work is still in progress. The 180° switching makes it possible to develop a genre of magneto-

elastic *memory* where bits are written entirely with voltage generated stress with no current flow. They are extremely energy-efficient.

In addition to memory devices, a universal NAND logic device has been proposed which satisfies all the essential characteristics of a Boolean logic gate. It is non-volatile unlike transistor based logic gates in the sense that that gate can process binary inputs and store the output (result) in the magnetization states of magnets, thereby doubling as both logic and memory. Such dual role elements can spawn non-traditional non-von-Neumann architectures without the processor and memory partition that reduces energy efficiency and introduces additional errors. A bit comparator is also designed, which happens to be all straintronic, yet reconfigurable. Moreover, a straintronic spin neuron is designed for neural computing architecture that dissipates orders of magnitude less energy than its CMOS based counterparts.

Chapter 1. Introduction

In digital electronics, there has always been a push for increasing the density of computing devices in a chip. This trend is captured by the famed Moore's law (Moore, 1965) that predicted that the density of transistors on a chip should double roughly every two years. However, sustaining this trend beyond the year 2020 requires a substantial reduction in the energy dissipated to switch a transistor and thus flip a binary bit. The quintessential complementary metal-oxide-semiconductor (CMOS) transistor operates by switching between the "ON" and "OFF" states by moving electrical charge in to or out of its active region. When carried out non-adiabatically, the energy dissipated in this process is at least NkTln(1/p), where N is the number of electrons (information carriers) moved in to or out of the device, k is the Boltzmann constant, T is the temperature and p is the "bit error probability" associated with erroneous switching of the device under the influence of thermal noise (Zhirnov et al., 2003; Salahuddin and Datta, 2007).

In contrast, if logic bits '0' and '1' are encoded in two stable magnetization orientations along the easy axis of a shape-anisotropic *single-domain* nanomagnet shown in Fig 1.1 (or the single domain magnetostrictive layer of a multiferroic nanomagnet), the energy dissipated during switching between these orientations to flip the bit could be only ~ *kTln(1/p)* (Salahuddin and Datta, 2007). This is because the 'information carriers' in single domain nanomagnets are electron spins (as opposed to electron charges in transistors) whose mutual exchange coupling ensures that they rotate in unison. Thus, in the limit of coherent magnetization rotation and switching, the energy dissipated in switching is independent of the number of spins. Thus, ~10^4-

10^5 spins comprising a single-domain nanomagnet collectively behave like a giant classical spin which serves as a single information carrier (Salahuddin and Datta, 2007; Cowburn et al., 1999) as illustrated in Fig 1.1. Hence, the nanomagnet dissipates only ~ *kTln(1/p)*. Therefore, for the same bit error probability *p*, the ratio of the minimum energy dissipated to switch a nanomagnet to that dissipated to switch a nanotransistor will be ~1/N << 1 if N is large. This makes a nanomagnet intrinsically a more energy-efficient switch than a transistor.

Therefore, nanomagnetic computing predicated on the use of a single-domain shape-

Fig. 1. 1 : The two stable magnetization orientations in a single domain ferromagnet shaped like an elliptical cylinder are shown with arrows.

anisotropic nanomagnet with two stable magnetization orientations as a binary switch offers extremely low energy dissipation to switch a bit. However, even though the *intrinsic* energy dissipation in a magnet is small, the *extrinsic* dissipation in clocking or switching the single domain nanomagnet between stable states can be large and completely overwhelm the intrinsic dissipation. The latter depends on the particular switching mechanism employed to switch magnetization. Many switching methodologies are woefully energy-inefficient and squander the intrinsic energy-advantage of the nanomagnet over the transistor. Switching can be accomplished through a variety of means such as with a magnetic field generated by an external electric current (Alam et al., 2010), applying a spin transfer torque by passing a spin polarized current through the magnet with the spin polarization in the direction of the hard axis (Slonczewski, 1996) or through a spin diffusion current (Behin-Aein et al., 2010), or by inducing domain wall motion

with a spin-polarized current (Yamanouchi et al., 2004; Fukami et al., 2009). But by and large, all these switching methodologies dissipate enormous amounts of energy in the switching circuit due to I^2R losses. As a result, they completely negate the energy advantage of the magnet.

A much more energy-efficient approach is to rotate the magnetization of a two phase multiferroic elliptical nanomagnet, comprising a magnetostrictive layer in elastic contact with a piezoelectric layer, with uniaxial mechanical stress generated by applying an electrical voltage across the piezoelectric layer (shown in Fig. 1.2) (Atulasimha, and Bandyopadhyay, 2010; Roy,
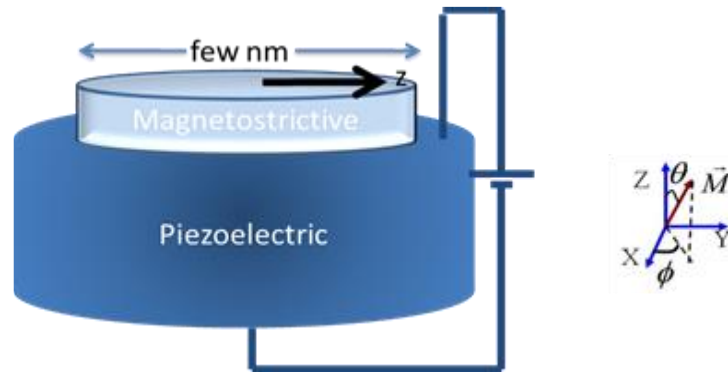
Fig. 1. 2 Strain-induced clocking of single-domain magnetostrictive nanomagnets elastically coupled to a piezoelectric substrate.

Bandyopadhyay, and Atulasimha, 2011).

It has been shown that an elliptical anisotropic multiferroic magnetostrictive nanomagnet can be switched reliably (> 99% probability) with stress between two stable states (rotation of magnetization by ~180°) (Roy, Bandyopadhyay, and Atulasimha, 2011) by withdrawing the stress at a precise juncture. Failure to withdraw at the right time will make the switching probability low (~50%). However, at room temperature, the magnetization experiences random thermal torques that make it impossible to time the stress withdrawal accurately. Because of the randomness of thermal noise, the withdrawal time will have a distribution of non-zero width, which means that one will require an extra feedback circuitry that tells the stress generator when

to withdraw the stress (Roy, Bandyopadhyay, and Atulasimha, 2013). This additional feedback circuitry adds to the total energy dissipation and hence makes the strategy unappealing.

In chapter 2, we describe how to accomplish magnetization switching between stable states in a memory device without any additional feedback circuitry and propose several device implementations. In chapter 3, we propose a universal NAND logic gate that satisfies all the essential characteristics of Boolean logic and is non-volatile. The non-volatility is a very desirable trait since it allows the device to double as both memory and logic. We then propose to implement a reconfigurable bit comparator using nanowire spin valves whose contacts are magnetostrictive nanomagnets. The advantage of this comparator over CMOS-based renditions is that it is more energy-efficient, but perhaps more importantly, it is non-volatile, meaning that the results of the comparison are stored in-situ in the comparator. Again, the non-volatility endows the device with the ability to "process and remember" which would elude traditional transistor based comparators that can only process and not remember   Chapter 3 also discusses an application of strain based switching for neural computing architecture and designs a straintronic spin neuron which is several orders of magnitude more energy-efficient than spin-transfer-torque based spin neurons recently proposed by others. In chapter 4, we report an experimental demonstration of complete 180° switching of a nanomagnet using stress alone. The device synthesis employed standard nanofabrication techniques.

Chapter 2. Hybrid spintronic and straintronic memory devices

In this chapter, we discuss several switching methodologies that utilize voltage generated strain as the primary propellant of switching the magnetization of a magnetostrictive nanomagnet. Multiple memory devices have been proposed and their energy efficiencies as well as switching probabilities have been calculated at room temperature through rigorous stochastic LLG simulations. Section 2.1 discusses a hybrid memory device based on a mixed mode switching scheme involving surface acoustic wave (SAW) generated strain and spin polarized current generated spin transfer torque (STT) that deterministically switches the magnetization by 180°. In section 2.2 we present a magneto-elastic memory device in which voltage-generated strain switches the magnetization between stable states that are separated by an angle as large as 135°. Section 2.3 elucidates complete 180° switching of magnetization with stress alone. This is an important advance since it was previously held that stress can switch magnetization by no more than 90^0. A 90^0 rotation is not enough; if we rotate the magnetization of a nanomagnet through 90^0, then we would have placed the nanomagnet in an unstable state equally separated from the two stables states that are anti-parallel and hence separated by an 180^0 angle. After stress removal, the magnetization would have equal probability of switching (going to the target state) and not switching (returning to the initial state) that defeats the purpose of switching. Therefore, the ability to rotate magnetization through complete 180^0 is crucial. This work has invented a scheme to achieve that and resulted in a patent filed with the USPTO.

In all subsequent chapters, we choose Terfenol-D as a magnetostrictive material unless otherwise stated. It has a large positive magnetostriction coefficient (λ_s = 600 ppm) with

saturation magnetization M_s = 8 x 10^5 A/m. The Gilbert damping coefficient $\alpha = 0.1$ in this

material and Young's modulus $Y = 80$ GPa.

2.1. Hybrid straintronic memory: Acoustically assisted spin transfer torque (STT) switching for non-volatile memory

The popular technology used for switching of nanomagnets is spin-transfer-torque (STT). STT is generated in a soft magnetic layer by passing a spin polarized current. The electrons in the spin polarized current impart their spin angular momenta to the resident electrons and make their spins turn in the direction of spin polarization. This rotates the magnetization of the soft magnet. The simplest implementation is a magneto-tunneling junction (MTJ) which has three layers – a hard magnet, a soft magnet and an intervening spacer layer. Current is injected from the hard layer to the soft layer after tunneling through the spacer. The injected current has the spin polarization of the hard magnet's magnetization and hence the soft magnet ultimately turns in the direction of the hard magnet's magnetization, assuming a "parallel" configuration. To make them anti-parallel, the voltage polarity is reversed. Now the soft magnet injects its majority spins into the hard magnet. This depletes the supply of majority spins in the soft magnet. Ultimately the majority spins become the minority and the magnetization of the soft magnet turns in the direction opposite to that of the hard magnet's magnetization, making the two anti-parallel.

Unfortunately, owing to the high critical current density and large resistance-area (RA) product of an MTJ, the energy dissipated for a particular switching event is very high (large dissipation through I^2R loss), where I is the charge current to produce the spin-polarized current.

We proposed a method to reduce charge current by introducing mixed mode switching in Ref (Biswas, Bandyopadhyay and Atulasimha, 2013). In this case, a global surface acoustic wave (SAW) is passed underneath a large number of magnets usually delineated on the top of a piezoelectric substrate (LiNbO3). SAW generates a strain pulse on the surface of LiNbO3 substrate.
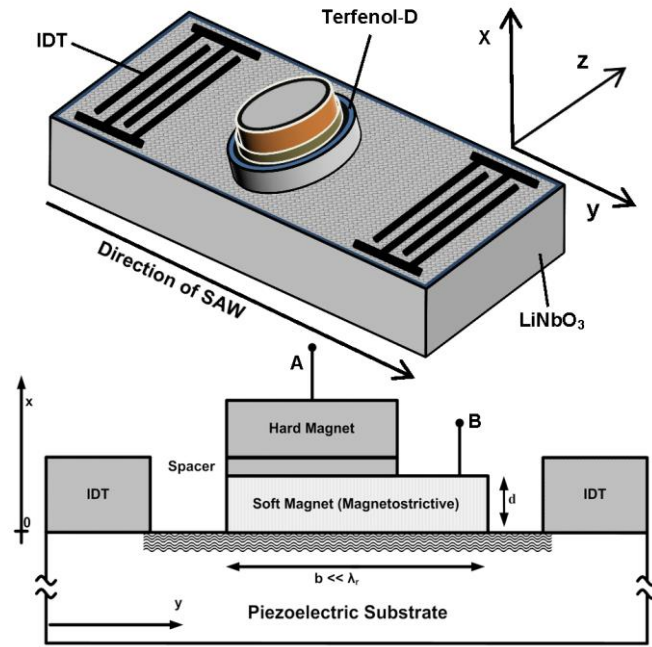
Fig. 2. 1 Schematic illustration of the system with interdigital transducers (IDTs) and a magneto-tunneling junction (MTJ), serving as a bit storage unit, placed between IDTs on a LiNbO$_3$ piezoelectric substrate. The soft layer of the MTJ is in contact with the substrate and is strained by the SAW. The resistance between the terminals A and B is used to read the bit stored (we assume that both magnets are metallic). For writing, a small spin polarized current is passed between the same two terminals during the appropriate cycle of the SAW. In this configuration, the reading and writing currents do not pass through the highly resistive piezoelectric, so the dissipation during the read/write operation is kept small. Bits are addressed for read/write using the traditional crossbar architecture. (Biswas, Bandyopadhyay, and Atulasimha, 2013).

Fig. 2.1 shows the schematic of the proposed device where two sets of interdigital transducers (IDTs) and the MTJ are delineated on top of a LiNbO$_3$ piezoelectric substrate. The velocity of SAW wave in LiNbO$_3$ is v_r = 3488 m/sec (Slobodnik, Conway and Delmonico, 1973). If we launch a wave of frequency 100 MHz, the corresponding wavelength λ_r is 34.88 µm.

7

Since the minor axis and the thickness of the soft magnetic layer in MTJ are b = 90 nm and d = 7 nm, the relations b<< λ_r and d<< λ_r are both satisfied. This allows us to assume that strain is uniformly distributed across the magnet, that shear stress has negligible effect on magnetization dynamics, that there is no shear lag effect (Thevenard et al., 2013) and that all stress is transferred from LiNbO$_3$ substrate to the nanomagnet.

Since the top of the magnet is not clamped, the normal component of stress can also be ignored. Therefore, one needs to consider only a uniaxial tangential component along the y-direction, i.e., the hard axis of the magnet. Spin polarized currents are passed through the magnetic layers using the terminals A and B. Consider the situation when the positive half cycle of the SAW generates tensile stress along the minor axis of the magnet and other half generates compressive stress. Tensile stress along the minor axis will rotate the magnetization from the easy to near hard axis (<90° rotation) for a positive magnetostrictive material like Terfenol-D with in the first quarter of the cycle and then during the second quarter spin polarized current is passed that generates STT torque (see the inset of the figure 2.2). Since STT torque can deterministically write bits (either '0' or '1'), utilizing the direction of current flow, the magnetization will be guided either over the hard axis to make a complete switching or back to original state determined by the current direction. Therefore, SAW does the heavy lifting but is not able to complete a switching event on its own.

In order to find the temporal evolution of the magnetization vector under the different torques mentioned, we solve the stochastic Landau-Lifshitz-Gilbert (LLG) equation under the macrospin assumption

$$\frac{dm(\text{t})}{dt} - \alpha\left(m(t) \times \frac{dm(\text{t})}{dt} \right) = \frac{-|\gamma|}{\mu_0 M_s \Omega}\left(\tau_{ss}(\text{t}) + \tau_{th}(\text{t}) + \tau_{sst}(\text{t}) \right)$$

(2.1)

Here, m(t) is the normalized equation are Gilbert damping coefficient α, gyromagnetic ratio of electron γ, saturation magnetization M_s, magnet's volume Ω and permeability of free space μ_0. Thermal torque τ_{th} has been modeled using the recipe discussed in Ref. (Roy, Bandyopadhyay, and Atulasimha, 2012). For the detailed calculations and the simulation procedure see Ref. (Biswas, Bandyopadhyay and Atulasimha, 2013). magnetization vector, τ_{ss}, τ_{th}, and τ_{sst} are the torques due to shape anisotropy energy of the soft magnet (Terfenol-D), random thermal noise at room temperature and spin-polarized currents through terminals A and B. Other parameters involved in the above equation are Gilbert damping coefficient α, gyromagnetic ratio of electron γ, saturation magnetization M_s, magnet's volume Ω and permeability of free space μ_0. Thermal torque τ_{th} has been modeled using the recipe discussed in Ref. (Roy, Bandyopadhyay, and Atulasimha, 2012). For the detailed calculations and the simulation procedure see Ref. (Biswas, Bandyopadhyay and Atulasimha, 2013).
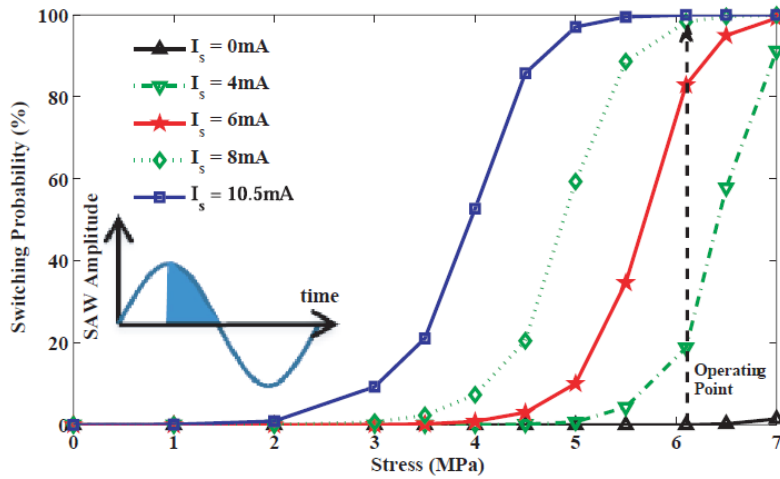
Fig. 2. 2 Probability of a magnet switching at room temperature in 5 nsec (half-period of the 100 MHz SAW) as a function of the peak stress generated by the SAW. The various curves are for different spin-polarized currents. Note that the probability of switching in the absence of spin polarized current ($I_s = 0$ mA) remains zero up to a peak stress of 6.1 MPa. The spin-polarized current is turned on for the latter half of the appropriate half-cycle of the SAW (2.5 nsec) as shown in the inset (shaded region) to write the bit. (Biswas, Bandyopadhyay, and Atulasimha, 2013).

9

In Fig. 2.2, the switching probability is plotted at room temperature as a function of peak stress generated by the SAW for various spin-polarized currents. First, we determine the maximum peak stress to be 6.1 MPa up to which then the probability remains <0.01% with SAW alone. This ensures that no unwanted bit flip occurs during the flow of SAW. Next, we find the value of current to be 10.5 mA in addition to SAW for which a bit switches with >99.99% probability at room temperature with in 5 ns. A stand-alone STT would require 23 mA current to achieve switching with probability >99.99% if one turns the current on for whole 5 ns. The energy dissipated to switch a magnet in this hybrid scheme has three contributions: energy dissipated in the magnet due to Gilbert damping, energy dissipated in the SAW, and the energy dissipated by the spin-polarized STT current. The contribution from the SAW is negligible since it is amortized over all the magnets affected by the SAW and the other contribution due to Gilbert damping is very small compared to the overwhelming $I_s^2 R t_s$ loss where I_s is the STT current, R is the resistance of the MTJ stack through which the current flows, and t_s is the quarter cycle time (2.5 ns) the SAW (Biswas, Bandyopadhyay and Atulasimha, 2013). With the addition of SAW I_s is reduced by a factor of 2.2 and t_s is decreased by a factor of 2, hence energy dissipation in hybrid mode switching (STT+SAW) is reduced by a factor of ~10.

2.2. Magneto-elastic memory: Switching the magnetization between two mutually perpendicular stable orientations and extension to stable orientations with angular separation > 90° resulting improved on-off ratio

Stress, by itself, can rotate the magnetization of a shape anisotropic nanomagnet by up to 90° with high probability as discussed in the introduction. In order to implement complete 180^0 switching with stress alone, one may think of a bi-stable nano-magnet in which magnetization

states are not separated by 180°, but by 90°, which is the maximum angle by which stress rotates the magnetization.   These idea was first conceived by Tiercelin et al. (Tiercelin et al., 2011; Giordano et al., 2012) where a small in-plane external magnetic field is applied along the hard axis of an elliptical nano-manget. External magnetic field dislodges the two stable states out of the easy axis (major axis of the ellipse) and places them such that the newly formed stable states are now 90° apart and remain in the plane of the magnet.
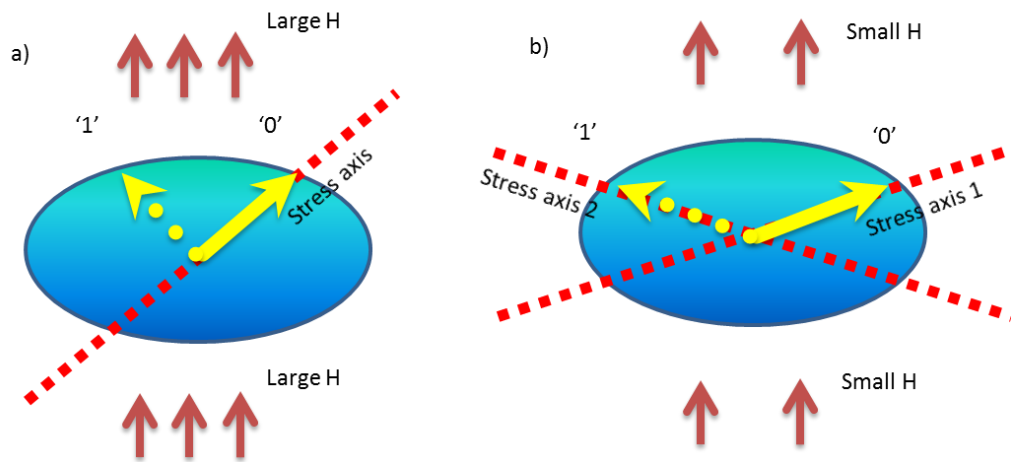
Fig. 2. 3 Use of a permanent bias field (H) applied along the minor axis of an elliptical nanomagnet to achieve stable states that are (a) mutually perpendicular (proposed by (Tiercelin et al., 2011); (b) make an angle > 90° (our proposal (Biswas, Bandyopadhyay and Atulasimha, 2014b)).

Fig. 2.3 (a) shows the proposed schematic of the scheme from Tiercelin et al. where a sufficiently large magnetic field brings the two stable magnetization to upper half of the ellipse in two adjacent quadrants literally making a 90° angle in between (Giordano et al., 2012). These two newly stable states encode bit '0' and bit '1' for a memory device. Stress is applied along one of the stable directions; in this figure it is along the direction in which bit '0' is encoded. If the nature of the stress happens to be compressive, for a nano-magnet with positive magnetostriction the magnetization rotates towards the direction of bit '1' irrespective of the initial state of magnetization since the latter direction becomes the only energy minimum

11

position for the magnet's plane. On the other hand, a tensile stress places the magnetization along the direction of bit '0' no matter what the stored bit was due to the same argument of only one energy minimum along bit '0'. The scheme, therefore, implements non-toggle switching for non-volatile memory application. Since tensile and compressive stress deterministically write the bits '0' and '1' respectively without any prior knowledge of the initial state, the above scheme does not require any read cycle to check for the type of stored bit before a write cycle appears. However, the scheme has a disadvantage when the stored bit is read with a magneto-tunneling junction (MTJ) that is vertically integrated above the nanomagnet. Different magnetization orientations in the nanomagnet result in different resistance values in an MTJ. The change in resistances should be high enough so that bits are clearly distinguishable. This distinguishability depends on the angular separation between the stable magnetization states of the nano-magnet. Consider a traditional MTJ that will use the magnetostrictive magnet as the soft magnetic layer (or free layer) and a synthetic anti-ferromagnet (SAF) as the hard magnetic layer (or fixed layer) with a tunneling layer in between. Let us assume that the magnetization of the fixed layer is anti-parallel to the direction that encodes bit '1'. Then the MTJ resistances with the soft layer's magnetization encoding bit '1' and bit '0' will bear a ratio $r = (1 - \eta_1 \eta_2 \cos \Theta)/(1 - \eta_1 \eta_2)$, where the η_i , i=(1,2) are respectively the spin injection/detection efficiencies of the two magnet interfaces of the MTJ and the angular separation between the two stable magnetization directions is Θ = 90° in the MTJ's free layer encoding the two bits. The maximum value of this ratio (assuming $\eta_1 = \eta_2 = 1$) is infinity, but realistically the η-s are about 0.7 at room temperature (Salis et al., 2005) and hence the ratio is ~2:1. Such a low ratio may make it difficult to distinguish between bits '0' and '1' in a noisy environment when the bits are read by measuring the MTJ resistance.

MTJ's resistance ratio can be improved if by some means the angle of separation between two magnetization states can be greater than 90°. In a recent paper (Biswas, Supriyo Bandyopadhyay and Atulasimha, 2014b), we showed that the ratio r can be improved without sacrificing any other metric if a smaller external static field is applied to bring the stable magnetization orientations into the upper half of ellipse (see figure 2.3 (b)) subtending an angle greater than 90° between them. In this case, to implement non-toggle switching, we introduce two pairs of electrodes (instead of just one) to generate stresses along two different directions in the magnet. Figure 2.3 (b) shows the schematic of the proposed device. A smaller static magnetic field makes the angular separation between the magnet's stable magnetization states Θ as large as 132°. Applying compressive stress along stress axis 1 will bring the magnetization to the magnetization direction of bit '1' while compressive stress in along stress axis 2 will bring the magnetization to the direction of bit '0' if magnetostriction of the nanomagnet is positive (the opposite will happen if the magnetostriction is negative). This idea of non-volatile non-toggle switching is recently applied to a different application like probabilistic computing other than memory (Khasnavis et al. 2015).

Fig. 2.4 shows the schematic of the proposed device. The PZT film has a thickness of $\sim$100 nm and is deposited on a conducting n^+-Si substrate. The elliptical nanomagnet has a major axis a = 110 nm, minor axis b = 90 nm, and thickness d = 9 nm. These dimensions ensure that the nanomagnet has a single magnetic domain (Cowburn et al. 1999) so that macrospin approximation remains valid. A small magnetic field (B = 8.5 mT) is applied along the in-plane hard axis of the magnet, which brings the magnetization stable states out of the major axis, but retain them in the plane of the magnet ($\phi = \pm90°$). The new stable states (the two degenerate

13

energy minima) are Ψ_I at $\theta = 24.09^\circ$ and Ψ_{II} at $\theta = 155.9^\circ$, where θ is the angle subtended by the magnetization vector with the z-axis (or major axis of the elliptical magnet). Therefore, the
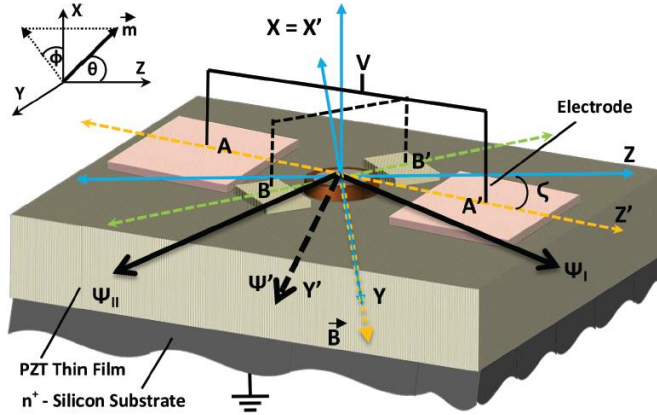
Fig. 2. 4 Schematic illustration of the system with two pairs of electrodes (AA′ and BB′) and the Terfenol-D nanomagnet delineated on top of a PZT piezoelectric layer. If the magnetization of the Terfenol-D nanomagnet was initially in the stable state Ψ_I (bit '0'), a voltage applied between the electrode pair AA′ and ground will switch its direction to the other stable state Ψ_{II} (writing the new bit '1'), while a voltage applied between the pair BB′ and ground will keep it in the original stable state Ψ_I (re-writing the old bit '0'). Thus, either bit can be written by activating the correct electrode pair, irrespective of what the initially stored bit was. (Biswas, Bandyopadhyay, and Atulasimha, 2014b).

angular separation between these states is $\sim 132^\circ$. The electrodes are delineated such that the line joining one pair subtends an angle $\zeta = 15^\circ$ with the z-axis and the line joining the other pair subtends an angle $\zeta = 165^\circ$. Therefore, the axis joining one pair lies close to one stable magnetization direction and the other lies close to the other stable magnetization direction. One pair of electrode pads has edge dimension of 170 nm and the other has edge dimension of 70 nm. These dimensions are needed to ensure the following: (1) the line joining the centers of each pair of pads lies close to one of the stable magnetization orientations, (2) the spacing between the facing edges of the pads in either pair is comparable to the pad's edge dimension and also the PZT film thickness, and (3) no two pads overlap (Cui et al. 2013).

Fig. 2.5 shows the potential energy profile of the nanomagnet in the magnet's plane ($\phi =$ 90°) as a function of the angle θ subtended by the magnetization vector with the major axis of the ellipse (z-axis). When no stress is applied and the static magnetic field is absent (curve I), the energy minima and the stable magnetization states lie along the major axis of the ellipse ($\theta = 0^\circ$, 180°) and the in-plane energy barrier separating them is ~145 kT at room temperature. Application of the static magnetic field along the minor axis (curve II) moves the energy minima and stable magnetization states out of the major axis to $\theta = 24.09^\circ$ and 155.9°, while reducing the in-plane energy barrier separating the stable states to 49.2 kT. Therefore, the probability of spontaneous magnetization flipping between the two stable states due to thermal noise (static error probability) is ~ $e^{-49.2}$ per attempt (Brown, 1963), leading to memory retention time (1/fo)$e^{-49.2}$ = 73 years, assuming the attempt frequency f_o is 1 THz (Gaunt , 1977). The new stable states are designated as Ψ_I (which encodes the binary bit '0') and Ψ_{II} (which encodes the binary bit '1').

Application of sufficient compressive stress along the line joining the electrode pair AA$'$ makes the potential profile monostable (instead of bistable; see curve III) and shifts the minimum energy position to Ψ', so that the system will go to this state, regardless of whether it was originally at state Ψ_I or Ψ_{II} . After stress removal, the magnetization will end up in the stable state Ψ_{II} (with very high probability at room temperature) since it is the energy minimum closer to Ψ' and getting to ΨI from Ψ' would have required transcending the energy barrier between Ψ' and Ψ_I . Thus, activating the pair AA$'$ deterministically writes the bit '1', regardless of the initially stored bit. Similarly, activating the other pair BB$'$ would have written the bit '0' (curve IV of Fig. 3.3).
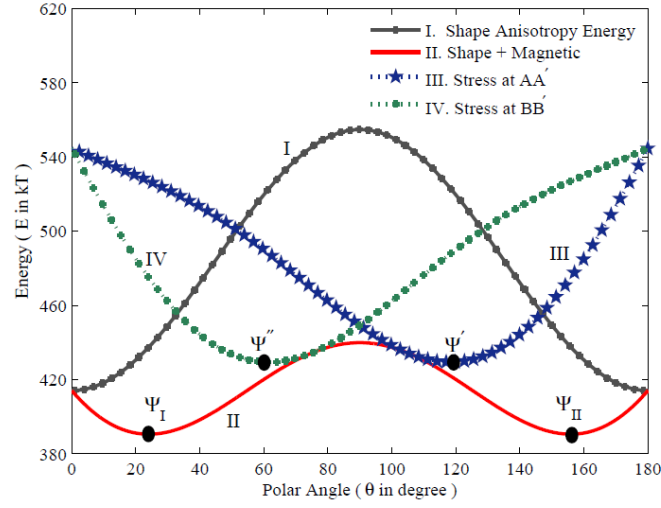
Fig. 2. 5 In-plane potential energy profile (azimuthal angle φ = 90°) of the nanomagnet in different conditions. Curve I shows the profile in the absence of any stress and the static magnetic field, where the energy minima are at θ = 0°, 180°. Curve II shows the profile in the presence of an in-plane magnetic field of 8.5mT along the nanomagnet's minor axis where the energy minima have moved to θ = 24.09° and at θ = 155.9°. Curves III and IV show the profile when a compressive stress of 9.2 MPa is generated by imposing a potential between the electrodes AA′ and the electrodes BB′, respectively. Note that stress makes the potential profile monostable, instead of bistable. (Biswas, Bandyopadhyay, and Atulasimha, 2014b)

In order to calculate the energy dissipated in writing a bit, as well as the probability with which the bit is written correctly in the presence of thermal noise, authors solve the stochastic Landau-Lifshitz-Gilbert equation given by (Biswas, Bandyopadhyay, and Atulasimha, 2014b)

$$\frac{dm(t)}{dt} - \alpha\left(m(t) \times \frac{dm(t)}{dt}\right) = \frac{-|\gamma|}{\mu_0 M_s \Omega}\left(\tau_{ss}(t) + \tau_{th}(t) + \tau_m(t)\right) \qquad (3.1)$$

where τ_{ss}, τ_{th}, and τ_m are the torques due to shape and stress anisotropy energy, thermal noise and external magnetic field respectively. The expressions for the τ_{ss} and τ_m can be written as

$$\tau_{ss} = \left\{ E_{\phi 1}(t) \sin \theta'(t) + E_{\phi 2}(t) \cos \theta'(t) \right\} \hat{\boldsymbol{\theta}} - \left\{ E_{s1}(t) \sin 2\theta'(t) + 2E_{s2}(t) \cos 2\theta'(t) + (3/2)\lambda_s \varepsilon(t) \, \text{Y} \, \Omega \sin 2\theta'(t) \right\} \hat{\boldsymbol{\phi}}$$

where

$$E_{\phi 1}(t) = \frac{\mu_0}{2} M_s^2 \Omega \left\{ \left(N_{d-xx} \cos^2 \zeta + N_{d-yy} \sin^2 \zeta \right) \sin 2\varphi'(t) - N_{d-xx} \sin 2\varphi'(t) \right\}$$

$$E_{\phi 2}(t) = \frac{\mu_0}{2} M_s^2 \Omega (N_{d-zz} - N_{d-yy}) \sin 2\zeta \cos \varphi'(t)$$

$$E_{s1}(t) = \frac{\mu_0}{2} M_s^2 \Omega \left(N_{d-xx} \cos^2 \varphi'(t) + N_{d-yy} \sin^2 \varphi'(t) \cos^2 \zeta - N_{d-yy} \sin^2 \zeta + N_{d-zz} \sin^2 \varphi'(t) \sin^2 \zeta - N_{d-zz} \cos^2 \zeta \right)$$

$$E_{s2}(t) = \frac{\mu_0}{4} M_s^2 \Omega (N_{d-zz} - N_{d-yy}) \sin \varphi'(t) \sin 2\zeta$$

and

$$\tau_m = \left\{ -M_s \Omega B \cos \zeta \cos \varphi'(t) \right\} \hat{\boldsymbol{\theta}} - \left\{ -M_s \Omega B (\cos \zeta \sin \varphi'(t) \cos \theta'(t)) \right\} \hat{\boldsymbol{\phi}} \tag{3.2}$$

θ'(t) and φ'(t) are, respectively, the instantaneous polar and azimuthal angles of the magnetization vector in the rotated frame, B is the magnetic field, M_s is the saturation magnetization of the magnet, $N_{d–xx}$, $N_{d–yy}$, and $N_{d–zz}$ are the demagnetization factors that can be evaluated from the nanomagnet's dimensions. We have shown that energy disspation is 718 kT while keeping the bit error probability as low as 2 x 10^{-6}. Interested readers can consult (Biswas, Bandyopadhyay and Atulasimha, 2014b) for details.

2.3. Pure Straintronic memory: Complete 180° switching of magnetization with stress alone

It is intuitive that a complete 180° angular separation between the '0' and '1' state would result in maximum ON-OFF ratio with a magneto-tunneling junction. However, due to the inherent shortcoming of stress of not being able to perform a complete rotation, it was a common belief that stress would never allow a 180° switching in an elliptical nanomagnet.

In a very recent paper (Biswas, Bandyopadhyay and Atulasimha, 2014a), we showed that this impasse can be overcome and a complete 180° rotation can indeed be accomplished with a voltage generated strain with a very high probability of success. Unlike the schemes in the previous sections, the new scheme uses no magnetic field where is required for the retention of magnetization along the major axes of the ellipse. Fig. 4.1 shows the device schematic of such a scheme with an MTJ structure placed on top of a PZT thin film. Two pairs of electrode pads are still in use and those are delineated on the PZT thin film such that pad pair 1 subtends an angle of 30° with major axis of the soft layer and pad pair 2 subtends and angle of 150°. In order to perform a complete switching stress is applied by activating one pad pair (say pad pair 1) first which rotate the magnetization to some angle (~ 60°) towards the other stable state. Then the stress applied upon the activation of other pad pair (say pad pair 2) and removal of other stress will rotate the magnetization by another ~60° towards the same direction. Finally, removal of stress will guide the magnetization to the other stable state, thus a complete switching is achieved. By altering the sequence of stress application, first activating pad pair 2 and then pad pair 1 will result in same 180° switching too. Therefore, for the same initial state if one stress sequence switches the magnetization by 180° in clockwise direction, other sequence switches the magnetization in anti-clockwise direction. The PZT film with the MTJ and electrode pad pair on top is deposited on a n+-Si substrate which is grounded. The PZT flim's thickness ~100 nm and electrode pad pair 1 has edge dimension of 80 nm and the pad pair 2 of 120 nm. We consider the elliptical nanomagnet has a single magnetic domain (Cowburn, et al., 1999) with a major axis a = 110 nm, minor axis b = 90 nm, and thickness d = 6 nm. These dimensions ensure that the nanomagnet has so that macrospin approximation remains valid. Figure 2.6 also shows the potential energy profile of the nanomagnet in the magnet's plane ($\phi = 90°, 270°$) as a function of

the polar angle θ subtended by the magnetization vector with the common major axis of the elliptical hard and soft layers (z-axis). The three potential energy profiles correspond to the
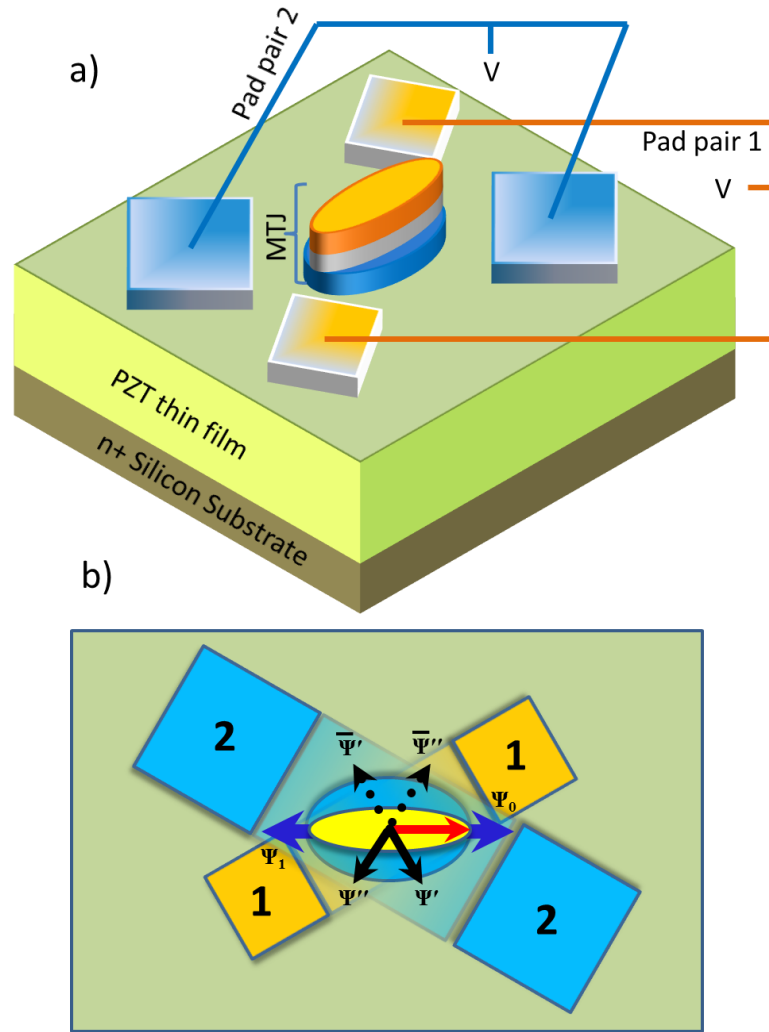
Fig. 2. 6 Schematic of memory element. (a) [Device schematic]. The PZT film has a thickness of 100 nm and is deposited on a conducting n+-Si substrate. It is poled with an electric field in the upward direction. The ratio of the distance between the facing edges of the electrodes to the electrode lateral dimensions is 1.67. (b) [2-dimensional view of the device]. The fixed magnetization orientation of the top (hard) magnet is denoted by the red arrow, and the two stable magnetization orientations of the bottom (soft) magnet are denoted by blue arrows. The MTJ resistance is high when the soft magnet's magnetization is aligned along Ψ_1 and the resistance is low when the soft magnet's magnetization is aligned along Ψ_0. Also shown are the orientations of the intermediate states Ψ', Ψ'', $\bar{\Psi}'$, $\bar{\Psi}''$. The eccentricity of the hard magnet is more than that of the soft magnet which helps to make the hard magnet "hard" and the soft magnet "soft".

situations when neither electrode pair is activated, electrode pair 1 is activated, and electrode pair 2 is activated.
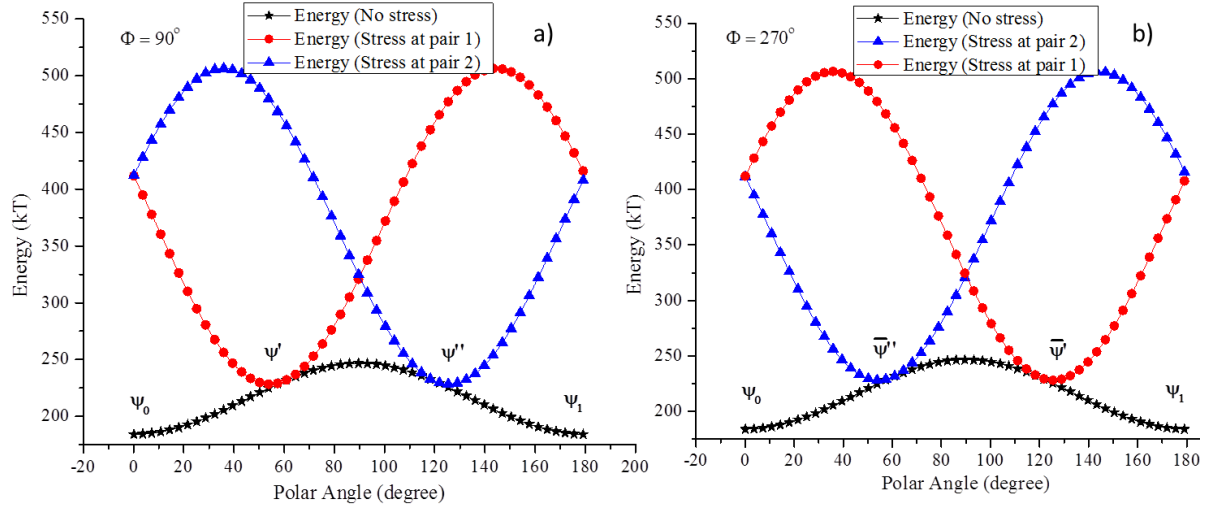
Fig. 2. 8 Potential energy profiles of a Terfenol-D magnetostrictive nanomagnet of stated dimensions when the magnetization vector is constrained to the plane of the magnet: (a) $\phi = 90^\circ$, and (b) $\phi = 270^\circ$. The three curves show the profiles when no electrode pair is activated, electrode pair 1 is activated and electrode pair 2 is activated. Activating electrode pair 1 creates global energy minima at Ψ' ($\phi = 90^\circ$) and $\overline{\Psi}'$ ($\phi = 270^\circ$), whereas activating pair 2, creates global minima at Ψ'' ($\phi = 90^\circ$) and $\overline{\Psi}''$ ($\phi = 270^\circ$). (Biswas, Bandyopadhyay, and Atulasimha, 2014a).

Consider the case when the magnetization of the nanomagnet is initially in the stable state Ψ_0 (initial stored bit is '0') and we wish to switch the magnetization from Ψ_0 to Ψ_1. We will first activate electrode pair 1 that will generate a compressive uniaxial stress along the line joining that electrode pair. This will rotate the magnetization vector to Ψ' since that corresponds to the only accessible global energy minimum (see the energy profile corresponding to $\phi = 90^\circ$ in Fig. 2.7).

The other global minimum at $\overline{\Psi}'$ is inaccessible owing to the energy barrier between Ψ_0 and $\overline{\Psi}'$ (see energy profile corresponding to $\phi = 270^\circ$ in Fig. 2.7; the peak of the energy barrier

20

separating Ψ_0 and $\bar{\Psi}'$ is located roughly at $\theta = 35°$). In other words, the magnetization will rotate clockwise instead of anti-clockwise in Fig. 2.6(b).

Next, de-activating pad pair 1 and activating pair 2 causes a uniaxial compressive stress component along the line joining pair 2 that will rotate the magnetization further in clockwise direction towards the new global energy minimum Ψ'', which is the only accessible one. Finally, removal of stress will drive the magnetization to Ψ_1 (writing the new bit '1') since it is the only accessible global energy minimum at that point. The other global energy minimum at Ψ_0 is inaccessible because of the energy barrier between Ψ'' and Ψ_0. The height of this energy barrier > 20 kT at room temperature and that prevents the magnetization from migrating to Ψ_0 instead of Ψ_1.

By applying stress i.e., by activating pad pairs in opposite sequence, first pair 2 and pair 1 will rotate the magnetization in counter-clockwise direction from Ψ_0 to Ψ_1 through the intermediate states $\bar{\Psi}''$ first and then $\bar{\Psi}'$ (see the energy profile corresponding to $\phi = 270°$). Therefore, no matter in which sequences the stress is applied by activating the electrode pads a complete flip occurs with high probability. Therefore, it is obvious that the present scheme has the shortcoming that it will erroneously write the wrong bit every time the stored bit happens to be the desired bit (since the stored bit is always flipped in the write step). Therefore, a write cycle must be preceded by a read cycle to determine the stored bit. If the stored bit is the same as the desired bit, no action is taken. Otherwise, the bit is flipped following the procedure just described. This requires an extra read cycle, but it also saves time and energy by obviating the write cycle whenever the stored and desired bits are the same. Since writing is both slower and more dissipative than reading, there may be an overall gain.

In order to check for dynamic error probability at room temperature under thermal perturbation, 10^6 switching trajectories generated by solving the stochastic Landau-Lifshitz-Gilbert equation in the manner of ref. (Biswas, Supriyo Bandyopadhyay and Atulasimha, 2014b) (magnetization orientation θ, ϕ versus time) with initial angles picked up from a Boltzmann distribution. All of them showed successful transition from θ ≈ 0° to θ ≈ 180° within 1.36 ns, implying that the switching failure probability is $< 10^{-6}$. The write error probability can be made even smaller if one after writing the bit, then reads it to verify if it was written correctly, re-writs it if written incorrectly, followed by another read and so on, until the bit is verified to have been written correctly. Alternately, one can always carry out a fixed number of write/verification cycles. The error probability after n such cycles is 10^{-6n} since it is the probability of having written the bit incorrectly *n* times in a row. Because it will be an overkill to reduce the write error probability to below the static error probability, which is the probability of spontaneous switching of the nanomagnet due to noise, just four (*n* = 4) read/verification cycles will be sufficient since the static error probability in the designed nanomagnet was 10^{-27}. The penalty associated with the 'repeated writing' approach to eliminate write errors is the *n*-fold increase in write time. Even if the bit was written correctly in the first attempt, one will still need three additional idle cycles since all bits are written simultaneously in parallel. This will increase the effective write time to 1.36 × 4 ns = 5.44 ns (again assuming that the read time is negligible compared to the write time), resulting in a clock rate of 180 MHz. For random access memory, this is still quite good.

The energy that dissipates in the device is due to twice of $(1/2)CV^2$ and due to Gilbert damping. By considering the larger electrodes of lateral dimension 120 nm with the PZT thickness 100 nm total dissipation due to CV^2 is 3896 kT where V is 112.5 mV. This dissipation

due to smaller electrodes (lateral dimension 80 nm) is 1733 kT. Mean internal dissipation due to Gilbert damping is found to be 514 kT thus making the total dissipation 6143 kT which is at least two orders of magnitude less than what spin-transfer-torque memory STT-RAM dissipates in a write cycle (Wang, Alzate and Khalili Amiri, 2013).

Chapter 3. Straintronic nanomagnetic logic devices (NML)

Since straintronic scheme of switching the magnetization in nanomagnets extremely energy efficient, we investigate the possibilities of making straintronic logic devices. In section 3.1 we show a universal NAND logic gate for Boolean computing that relies on strain based switching. A reconfigurable bit comparator has been proposed in section 3.2 by combining the physics of electron transport in nano-wire spin valve, magneto-elastic switching of nanomagnets with strain and magneto-tunneling junction (MTJ). Section 3.3 talks about a spin neuron for non-Boolean brain inspired computing.

3.1. Boolean NAND logic devices

A universal logic gate, that possesses all essential characteristics such as concatenability, non-linearity, isolation between input and output, gain, universal logic implementation and scalability along with ultralow energy delay product while maintaining high switching probability, is extremely desirable for the replacement of CMOS technology with nanomagnetic logic. Several efforts have been attempted with dipole coupled magnets (Cowburn, R. P. and Welland, M. E. 2000), with single MTJ (Ney et al. 2003), and with spin current (Behin-Aein et al. 2010). Dipole coupled architectures not only tend to be error-prone in the presence of thermal noise, (Salehi Fashami et al., 2013, Salehi Fashami, Atulasimha, Bandyopadhyay 2013), but they are also not robust against misalignments due to fabrication imperfections (Bandyopadhyay and Cahay, 2009). Moreover, the first two papers do not fulfill the requirement of concatenation for a universal logic gate whereas the third paper although fulfill all the requirements does not study error probability of the gate under room temperature. In a very recent paper Ref. (Biswas, Atulasimha and Bandyopadhyay, 2014), we proposed an error resilient non-volatile straintronic

universal NAND gate that fulfills all essential characteristics of a logic gate and possesses ultralow energy delay product of 2.78×10^{-26} J-s while maintaining bit error rate $< 10^{-8}$.

Fig. 3.1 shows the schematic of the single device that works as a logic unit. A pair of electrodes and a MTJ are delineated on the top of a PZT thin film while the whole structure is deposited on conducting n+-Silicon substrate. An in-plane magnetic field ensures the ~90° separation between stable states (ψ_0 and ψ_1) in the soft layer of the magnet as we discussed in section 2.2 (Tiercelin et al, 2011) . Compressive stress at EE′ will rotate the magnetization to ψ_0 while tensile stress will bring the magnetization to ψ_1. The magnetization of the hard layer is implemented with SAF and permanently magnetized along ψ_f opposite to ψ_1. Method of stress generation is same as we have discussed in section 2.3 (Cui et al., 2013) hence not repeated here. Let us encode bit '1' with the magnetization state of ψ_1 (high voltage state as V_o) and bit '0' with ψ_0 (low voltage state as $V_o/2$). Resistors and current/voltage sources ensure that the all logic operation in the NAND gate is achieved. Fig. 3.1 shows all four operations for the gate which we discuss below (Biswas, Atulasimha and Bandyopadhyay, 2014).

Before any gate operation a RESEST is performed by setting both inputs to $V_o/4$ that leaves the gate at high voltage state V_o (see Fig. 3.1). The bias voltage V_{bias} is turned on and set to $2V_o/3$. Hence, the potential difference applied across the thickness of the PZT film under E (or E′) is $-5V_o/12$. This produces 37.5 MPa tensile stress along E-E′ (compressive stress perpendicular to it) and deterministically rotates the magnetization to the state ψ_1 which produces an output voltage of V_o. Therefore, after every RESET operation MTJ reads bit '1'. Let us discuss the other logic operations. When both the inputs are low, potential difference across the PZT is $-V_o/6$ (corresponding tensile tress of 15 MPa). This stress will not change the state of magnetization from ψ_1 and the output continues to remain V_o representing bit '1'.
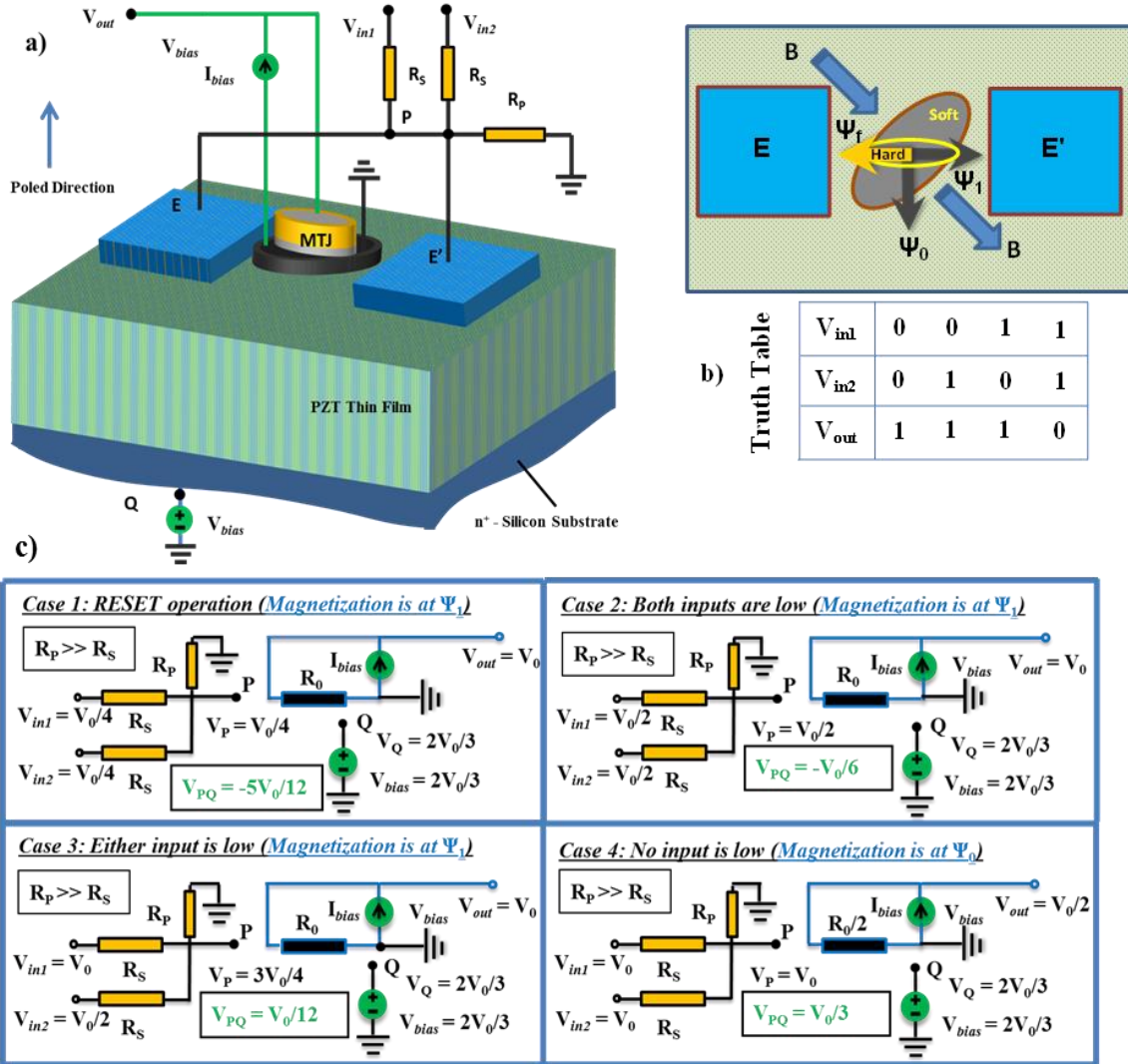
Fig. 3. 1 Straintronic-MTJ based universal logic gate that satisfies all characteristics for logic (top) Elevation view of device schematic (bottom) equivalent circuit representation of the gate (Biswas, Atulasimha, Bandyopadhyay, 2014).

When one of the inputs is high, potential difference across the PZT is lowered to $+ V_0/12$ generating a stress (compressive) of -7.5 MPa (see figure 1.19). This stress is not high enough to rotate the magnetization from its initial states that is high state and thus output remains high representing bit '1'. Subsequently inputs are applied to the gate (bits '1' and '0' correspond to input level V_0 and $V_0/2$ respectively). When both the inputs are high, the potential difference becomes $+V_0/3$ across the thin film underneath E (or E′) resulting in a -30 MPa compressive

26

stress to rotate the magnetization to ψ_0. The output voltage thereby drops to $V_o/2$ implementing a log logic state for bit '0' (see Fig. 3.1). Thus, a NAND gate is implemented. When we turn off all the bias voltage, there is no stress on the magnet, hence both ψ_0 and ψ_1 are stable (Tiercelin et al., 2011) due to the permanent bias magnetic field applied along the hard axis of the elliptical nanomagnet. Thus, '0' and '1' states (ψ_o and ψ_1 respectively) are stable and this implementation is non-volatile.

Finally, for these gates to be concataneble, the '0' and '1' states (ψ_0 and ψ_1 magnetization states of the MTJ respectively) should produce an output voltage of $V_o/2$ and V_o respectively. For more elaborate discussion please see Ref. (Biswas, Atulasimha, Bandyopadhyay, 2014).

3.2. Reconfigurable bit comparator

In this section, we propose a reconfigurable bit comparator implemented with a nanowire spin valve whose contacts are magnetostrictive and possess bistable magnetization. Reference and input bits are "written" into the magnetization states of the two contacts with electrically generated strain and the spin-valve's resistance is lowered if the bits match. Multiple comparators can be interfaced in parallel with a magneto-tunneling junction to determine if an N-bit input stream matches an N-bit reference stream bit by bit.

Fig. 3.2 (a) shows the schematic of an N-bit comparator fabricated on a conducting n+- Si substrate and a piezoelectric layer. A single bit comparator block is shown in the left panel of Fig. 6.1 (b) and consists of a nanowire "spin valve" whose two ferromagnetic contacts are two-phase multiferroics each consisting of a magnetostrictive material deposited on a piezoelectric layer.
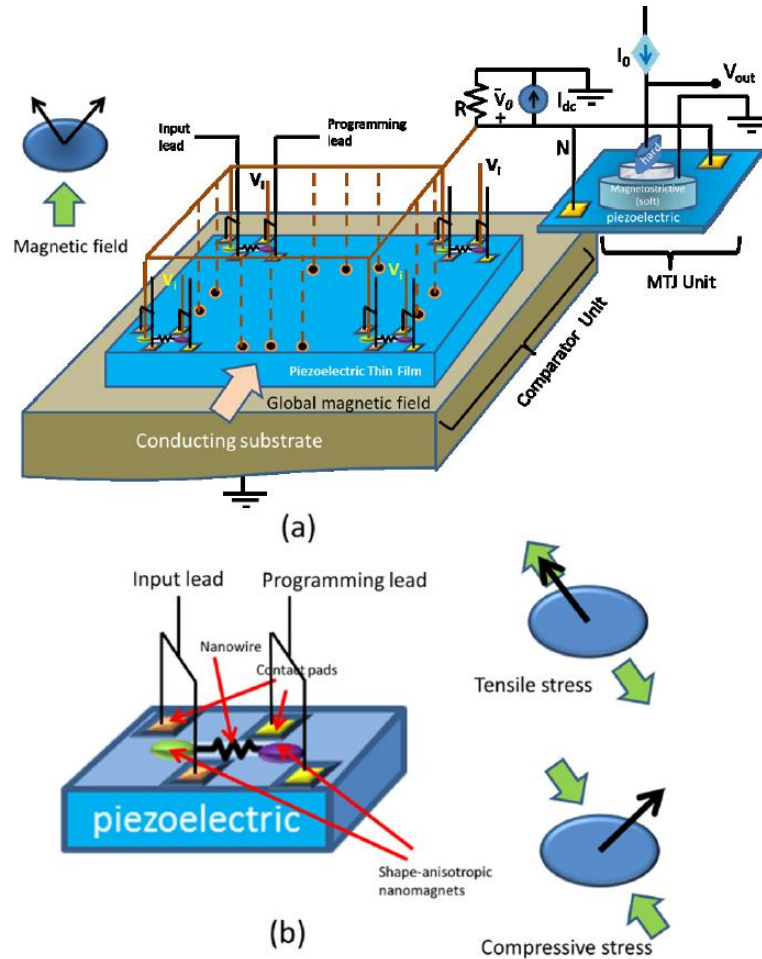
Fig. 3. 2 A straintronic-spintronic multi-bit comparator integrated with a magneto-tunneling junction whose resistance indicates whether the input and reference bit streams match bit by bit. The MTJ unit and the comparator unit share the same (grounded) conducting substrate although that has not been shown explicitly in the figure for the sake of clarity. (b) [Left panel] A single bit comparator unit showing the nanowire spin valve with magnetostrictive contacts fabricated on a piezoelectric layer. The programming and input leads are shown. [Right panel] Uniaxial tensile stress applied along one stable orientation of the nanomagnet takes the magnetization to that orientation while compressive stress takes the magnetization to the other orientation. (Biswas, Atulasimha and Bandyopadhyay, 2015).

A global static magnetic field is directed along the minor axes of the magnetostrictive contacts to make the magnetization orientation bistable. Two pairs of electrically shorted electrodes are also delineated on the piezoelectric film, with each pair flanking a magnetostrictive contact. Application of a potential (of appropriate sign and magnitude) between an electrode pair and the underlying grounded n+-Si substrate selectively determines either stable state. When the

28

potentials applied in both the reference and the input contacts are of same type (meaning the identical bits are received), both contacts form parallel magnetization configuration, resulting in a low resistive path from one contact to the other through the spin valve. When the potentials are of different types, the magnetizations in the contacts remain perpendicular to each other providing a high resistive path. Voltage at the across the road resistance R for a N-bit comparator unit will be given as

$$V_0 = V_I \sum_{n=1}^{N} \frac{R_n}{R_n + r_n},$$

(6.1)

where $R_n = R \parallel r_1 \parallel r_2 \parallel \cdots \parallel r_{n-1} \parallel r_{n+1} \parallel \cdots \parallel r_N$ and r_n is the resistance of the n-th spin valve. Note that the voltage V_0 is applied at the MTJ electrodes. There is a positive threshold voltage V_{th} which, when applied at these electrodes, will generate enough compressive stress in the soft layer of the MTJ to rotate its magnetization from the initial ("reset") orientation to the other stable orientation that is roughly perpendicular to the magnetization of the hard layer. This will abruptly take the MTJ to the low-resistance state and reduce the resistance by a factor of $1= (1 - \eta_1\eta_2)$ from the initial high-resistance state. The MTJ is biased by a constant current source I_0 which generates an output voltage $V_{out} = I_0R_{MTJ}$, where R_{MTJ} is the MTJ resistance. If $V_0 \geq V_{th}$, then V_{out} is low; otherwise, V_{out} is high. However, V_0 might be far away from V_{th} value but the former can be fine-tuned with a variable current source I_{dc} as shown in Fig. 3.2 (a). We determine the transfer characteristic of the soft magnetic layer of the MTJ at room temperature (see Fig. 3.3). At room temperature, there will be a broadening of the threshold to $V_{th} \pm \Delta V=2$. Therefore, to make the scheme work at room temperature, we ensure that if even one bit does not match, the resulting V_0 appearing across the resistor R is considerably less than $V_{th} - \Delta V=2$. This can be ensured by choosing V_I , R, I_{dc} and the spin valve resistances in the low- and high-

29

resistance states judiciously. We designed a 16-bit reconfigurable parallel comparator satisfying all the criteria mentioned above (Biswas, Atulasimha, Bandyopadhyay, 2015).
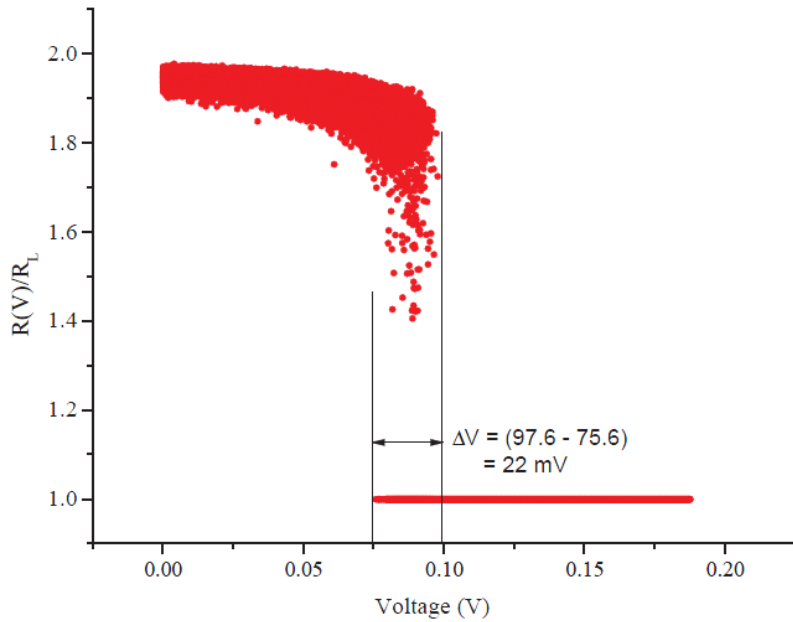
Fig. 3. 3 Switching characteristic of the MTJ switch R(V) versus V in the presence of thermal noise at room temperature. This plot is generated by simulating 10^5 switching trajectories to find the thermal spread in the switching threshold. (Biswas, Atulasimha and Bandyopadhyay, 2015).

We found that the system is robust against thermal noise at room temperature and it can operate at ~294 MHz while dissipating at most ~19 fJ per cycle.

3.3. Non-Boolean logic devices: straintronic spin neuron

Inspired from a human brain's capability of performing immense parallel operation with very low energy dissipation, a neural computing architecture has been proposed recently. 'Neurons' are the central units of computation which are usually connected to each other and to external stimuli through programmable synapses. However, neurons are implemented with CMOS operational amplifiers and usually consume exorbitant amount of energy. An alternative

is an energy efficient spin neuron implemented with nanomagnets driven by spin transfer torque (STT) generated from spin polarized current. When the latter happens to be far more energy efficient than CMOS based counterpart, its room temperature operation has not been properly studied. We propose a straintronic spin neuron that will be operated with voltage generated strain unlike the current. We show that our neuron is even more energy-efficient than STT based neuron with better thermal stability.
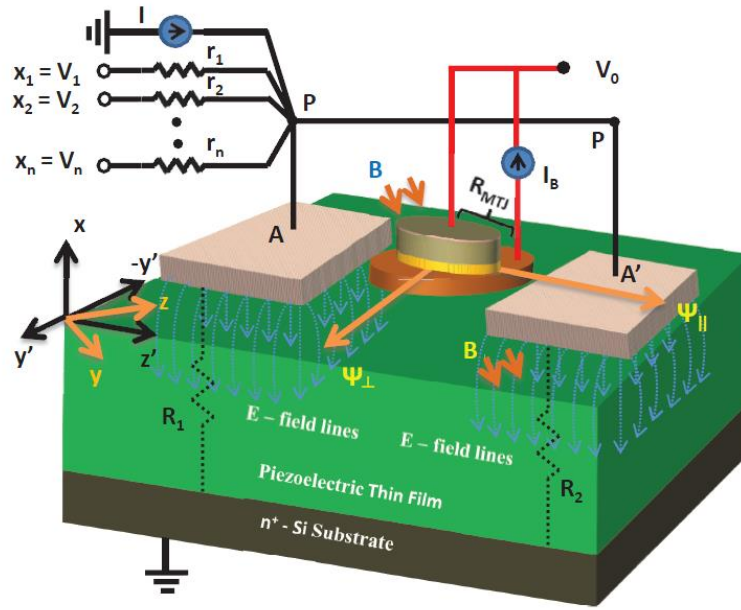
Using superposition

$$V_P = \sum_{i=1}^{N} w_i V_i + b$$

$$\text{where } w_i = \frac{R_1 \| R_2 \| r_1 \| r_2 \| \bullet\bullet\bullet \| r_{i-1} \| r_{i+1} \| \bullet\bullet\bullet \| r_N}{R_1 \| R_2 \| r_1 \| r_2 \| \bullet\bullet\bullet \| r_{i-1} \| r_{i+1} \| \bullet\bullet\bullet \| r_N + r_i}$$

$$\text{and } b = I(R_1 \| R_2 \| r_1 \| r_2 \| \bullet\bullet\bullet \| r_i \| \bullet\bullet\bullet \| r_N)$$

$$V_0 = I_B R_{MTJ} = f(V_P) = f\left(\sum_{i=1}^{N} v_i + b\right) = f\left(\sum_{i=1}^{N} w_i V_i + b\right)$$

$$\Rightarrow O = f\left(\sum_{i=1}^{N} w_i x_i + b\right)$$

Fig. 3. 4 Schematic of a straintronic spin-neuron implementing a step transfer function. The artificial synapses are realized with the passive resistors $r_1 \cdots r_n$. (Biswas, Atulasimha and Bandyopadhyay, 2015a)

Fig. 3.4 shows the schematic of a straintronic neuron connected to other neurons through programmable synapses (represented as resistors in Fig. 3.4) and an external bias. When the sum of the voltages at node P exceeds a critical value (corresponding to a critical stress of soft

magnetic layer in the MTJ) the output voltage V_0 changes abruptly. This mimic the behavior of a neuron's firing which is usually formalized by a step transfer function given as

$$O = f\left(\sum_i w_i x_i + b\right),$$ (7.1)

where x_i-s are the inputs to the neurons, w_i-s are the weightages of the synapses, b represents an external bias and f is some non-linear function. The inset in Fig. 3.4 shows the implementation of above equation for our straintronic spin neuron. We show that this neuron dissipates only 8.83 aJ energy at 0 K temperatures which is four orders of magnitude less than CMOS based neurons and 29,445 times less than a STT-based spin neuron. We further compare the transfer characteristic of both strain-based and STT-based neurons at 0 K and at room temperature. Fig. 3.5 shows all four different criteria. It is clearly shown that both of the neurons deviate from their sharp transfer characteristics to a broadened transitional behavior at the critical voltage/current value. These broadenings are inevitable since thermal noise at room temperature budges the magnetization around its equilibrium. However, the percentage of broadening in critical value (current) for the STT-based neuron is way higher than that (broadening in critical voltage) of the strain-based neuron which makes the viability of the former at room temperature questionable .
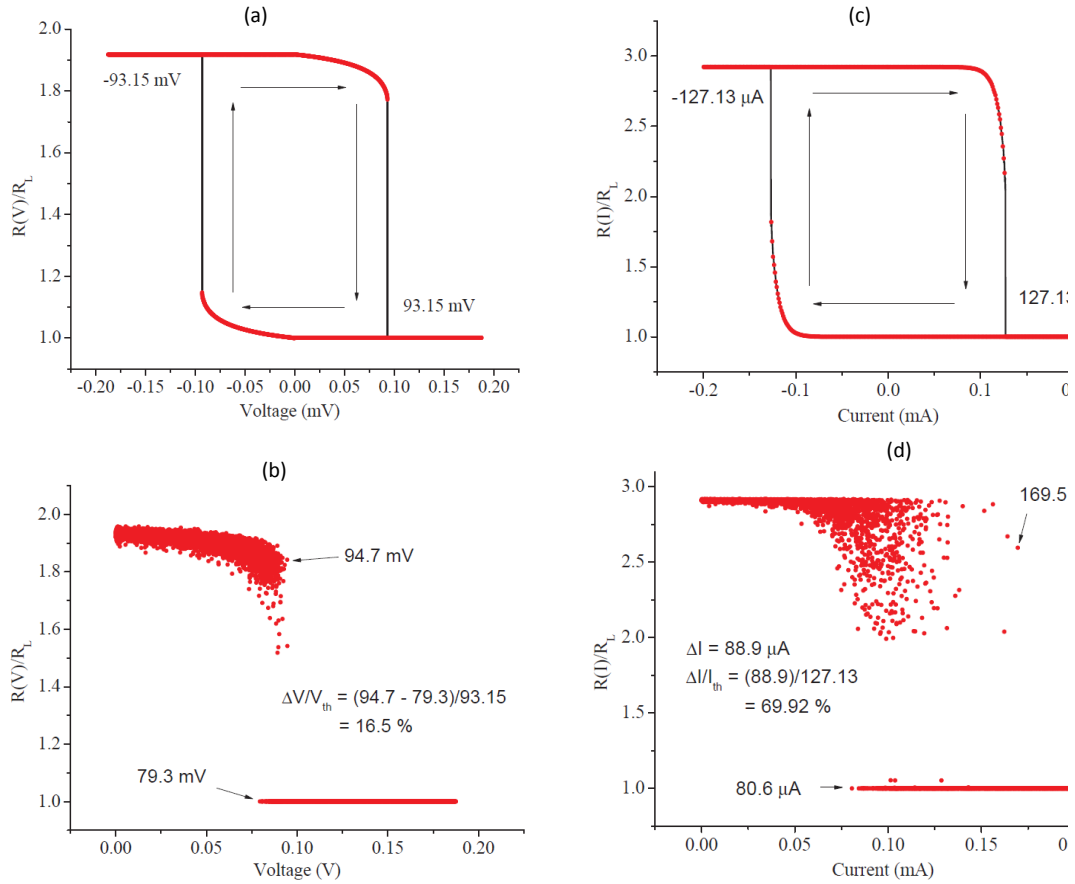
Fig. 3. 5 The transfer function (or firing behavior) for a straintronic spin neuron at 0 K. When the voltage appearing at node P (in Figure 1) due to weighted inputs and bias is V, the resistance of the MTJ is R(V). The low resistance is RL (b) Transfer characteristic (or firing behavior) for the straintronic spin neuron at room temperature in the presence of thermal noise. Results are shown for positive threshold only since no additional information can be gleaned from the negative threshold segment. Since the simulation is terminated immediately upon completion of firing, no fluctuations in the transfer characteristic are visible in the low-resistance state. (c) The transfer characteristic (or firing behavior) for a STT-based current driven spin neuron at 0 K. R(I) is the resistance of the MTJ when the total current injected into the soft layer (due to weighted inputs and bias) is I and RL is again the low resistance of the MTJ. (d) Transfer characteristic (or firing behavior) for the current-driven spin neuron at room temperature in the presence of thermal noise. (Biswas, Atulasimha and Bandyopadhyay, 2015a)

33

Chapter 4. Experimental demonstration of all-straintronic memory device: a complete 180º switching

In this chapter, we demonstrate a complete 180º switching scheme for a non-volatile memory proposed in section 4. We delineate elliptical magnetostrictive Co nanomagnets on (001) $Pb(Mg_{1/3}Nb_{2/3})O_3$-$PbTiO_3$ (PMN-PT) 70/30 substrate.
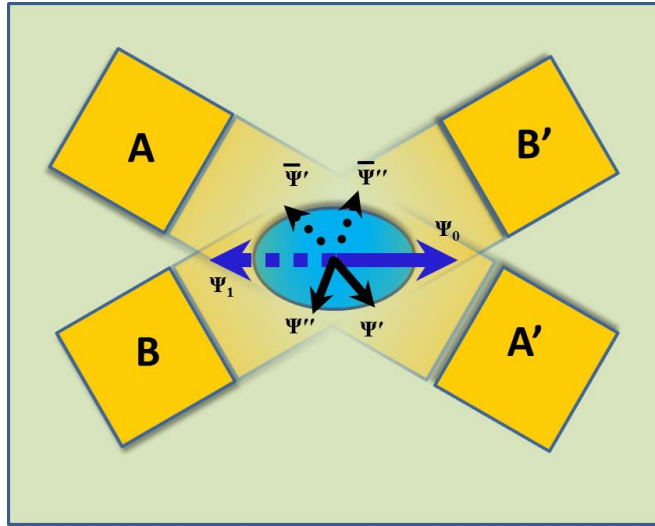
Fig. 4. 1 Top view of the device. Two pairs of electrodes, the line joining one pair makes an angle of 30 degree with the major axis and the other pair makes an angle of 150 degree.

Fig. 4.1 shows a schematic (top view) of this experimental setup where two pairs of metal electrodes are also deposited on PMN-PT substrate (of dimensions 10 mm × 10 mm × 0.5 mm) such that the line joining one pair of electrodes, AA′ makes an angle of 150º with the major axis of the magnet and the other pair BB′ makes an angle of 30º with the same major axis. We have deposited nanometer sized Co magnets of different dimensions using standard e-beam lithography, metal evaporation and lift-off. We can apply a strong external magnetic field to initialize all the domains in either direction (Ψ_0 or Ψ_1) along the major axis. Let us assume that the magnetizations in those domains are along Ψ_0 initially. When a voltage is applied between

one pair of electrode (say AA′) and grounded substrate, the magnetizations in majority number of domains will rotate from easy axis to an intermediate state called $\overline{\Psi}''$. Then we apply voltage to the other pair BB′ and simultaneously remove the voltage from AA′, the magnetizations will align themselves along $\overline{\Psi}'$. Finally, removal of the voltage from BB′ will guide the magnetizations towards Ψ_1. Since Co has a negative magnetostriction coefficient $((3/2)\lambda_S = -34 \times 10^{-6}$, (Long, 2008)), a tensile stress applied along the line joining electrode pair AA′ will place the magnetization normal to that line.

In order to fabricate the device we first poled the PMN-PT piezoelectric substrate along the direction perpendicular to the plane using a high electric field (0.6 MV/m). Next, we applied photoresist (SPR3012) using spin coating followed by lithography and development of the resist. Then, 70 nm thick Au electrodes (lateral dimensions of 0.4 mm $\times$ 0.4 mm) were deposited using electron-beam evaporation. Finally a lift-off process was performed to get rid of the resist and metal on top of resist. Then electron beam lithography was performed to deposit Co nanomagnets. Two layers of e-beam resist PMMA – Poly(methyl methacrylate) with different molecular weights (495K PMMA and 950K PMMA; 2% Anisole) were spin coated at 2500 rpm in two steps. The resists were baked at 115° Celsius for 2 minutes in each step. The sample was then exposed under electron beam from a Hitachi SU-70 SEM with a Nabity attachment using an accelerating voltage of 30kV and a beam current of 60 pA. Subsequently, the resists were developed in MIBK:IPA (1:3) [(methyl isobutyl ketone: isopropyl alcohol)] solution for 90 seconds followed by cold IPA rinse. Nanomagnets (thickness of 9 nm) are then deposited using electron beam evaporation at a base pressure of 2 x 10^{-7} torr with a Ti adhesion layer (thickness of 4 nm). A lift off process was conducted for removing the resist and metal to get the final device structure (see Figure 4.2).

Fig. 4. 2 Experimental setup before application of stress. Copper tape has been used for external contact with the bigger Au electrodes that are deposited on the PMN-PT substrate.

In order to study magnetization switching due to the application of voltage generated stress, we at first initialize the elliptical nanomagnets along the major axis of the ellipse with an external magnetic field of 1.5 Tesla. Following this, a vertical electrical field of 0.6 MV/m (300 Volts over a thickness of PMN-PT substrate of 0.5 mm) was sequentially applied with one pair at first and then with the other pair while removing the field from the first pair. This should correspond to uniaxial tensile stress of 125.8 MPa due to one electrode pad in an ideal case if we neglect the deformation of the magnet along the direction perpendicular to the tensile stress which would otherwise generate an additional compressive stress of 40.2 MPa in that direction. Here, we consider that the d_{31} coefficient of PMN-PT is 1000 pm/V and Young's modulus of Co is 209 GPa. Furthermore, there may be stress concentration due to non-uniformities, cracks and defects in the substrates. With stress concentration, some magnets might see excess stress. A more accurate stress profile can be generated using finite element method (FEM) analysis with

the commercially available package COMSOL. However, this is not the focal point of this thesis and will be deferred for later discussion.

Pre-stress and post-stress magnetic force microscopy (MFM) were performed to determine the magnetization states. MFM images show the evidences of 180° switching of nanomagnets in multiple cases (see Fig 4.3 to Fig. 4.7).
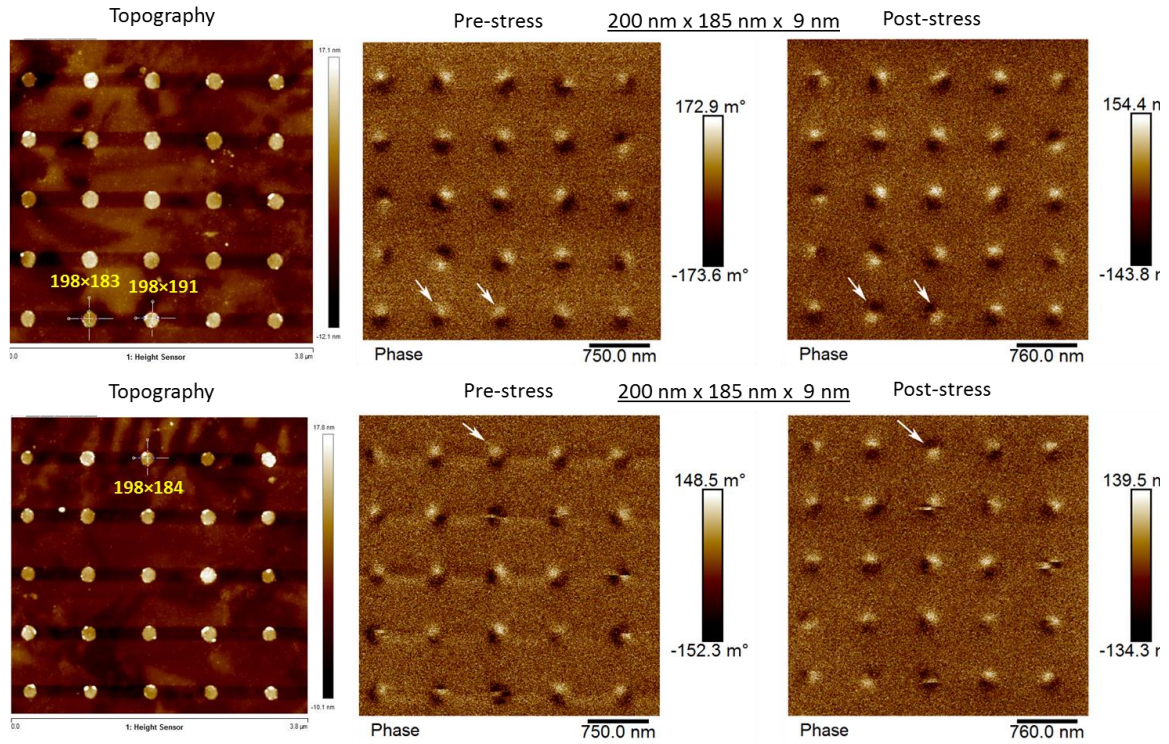
Fig. 4. 3 Pre-stress and post-stress MFM images for dimension of 200 nm $\times$ 185 nm $\times$ 9 nm in different location on the PMN-PT substrate. Two magnets switched by ~180° in one location (top subfigure) and one switched in the other (bottom subfigure) by ~180°. Actual dimensions measured for the switched magnets are 198 nm $\times$ 183 nm $\times$ 9 nm & 198 nm $\times$ 191 nm $\times$ 9 nm for the top location and 198 nm $\times$ 184 nm $\times$ 9 nm for the bottom location. White arrows indicate the switched nanomagnets after the application of stress. (Lateral dimensions shown in figures are in nanometers).
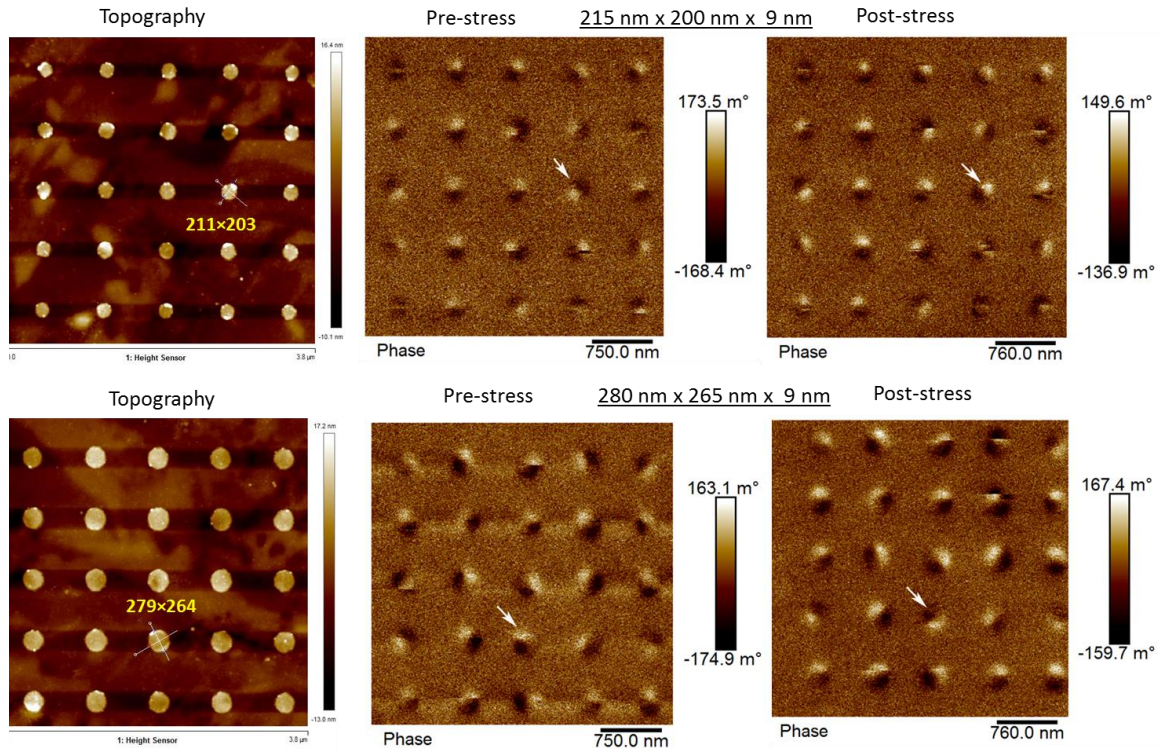
Fig. 4. 4 Pre-stress and post-stress MFM images for dimensions of 215 nm × 200 nm × 9 nm (top two subfigures) and 280 nm × 265 nm × 9 nm (bottom subfigures) on the PMN-PT substrate. One magnet switched by ~180° in one location (top subfigure) and one switched in the other (bottom subfigure) by ~170°. Actual dimensions measured for the switched magnets are 211 nm × 203 nm × 10 nm & 279 nm × 264 nm × 9 nm for the top and for the bottom respectively. White arrows indicate the switched nanomagnets after the application of stress. (Lateral dimensions shown in figures are in nanometers).
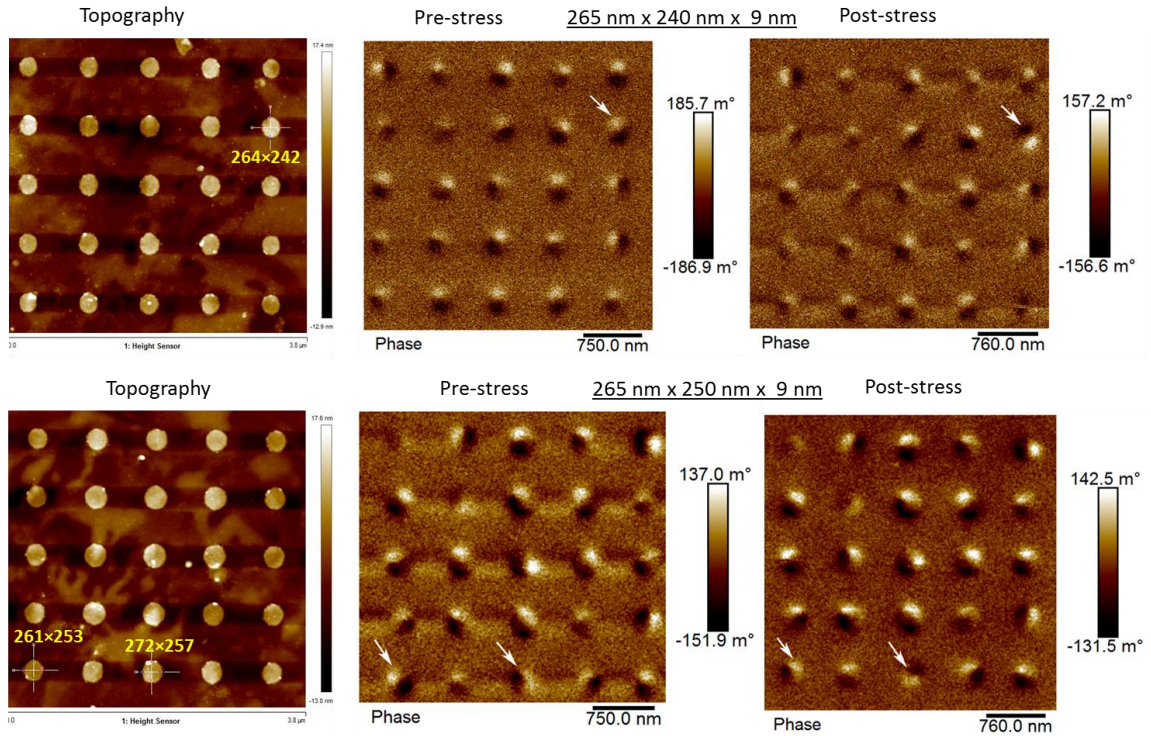
Fig. 4. 5 Pre-stress and post-stress MFM images for dimensions of 265 nm × 240 nm × 9 nm (top two subfigures) and 265 nm × 250 nm × 9 nm (bottom subfigures) on the PMN-PT substrate. One magnet switched by ~180° in one location (top subfigure) and two switched in the other (bottom subfigure) by ~170°. Actual dimensions measured for the switched magnets are 264 nm x 242 nm x 9 nm for the top and 261 nm × 253 nm × 8 nm & 272 nm × 257 nm × 10 nm for the bottom respectively. White arrows indicate the switched nanomagnets after the application of stress. (Lateral dimensions shown in figures are in nanometers).
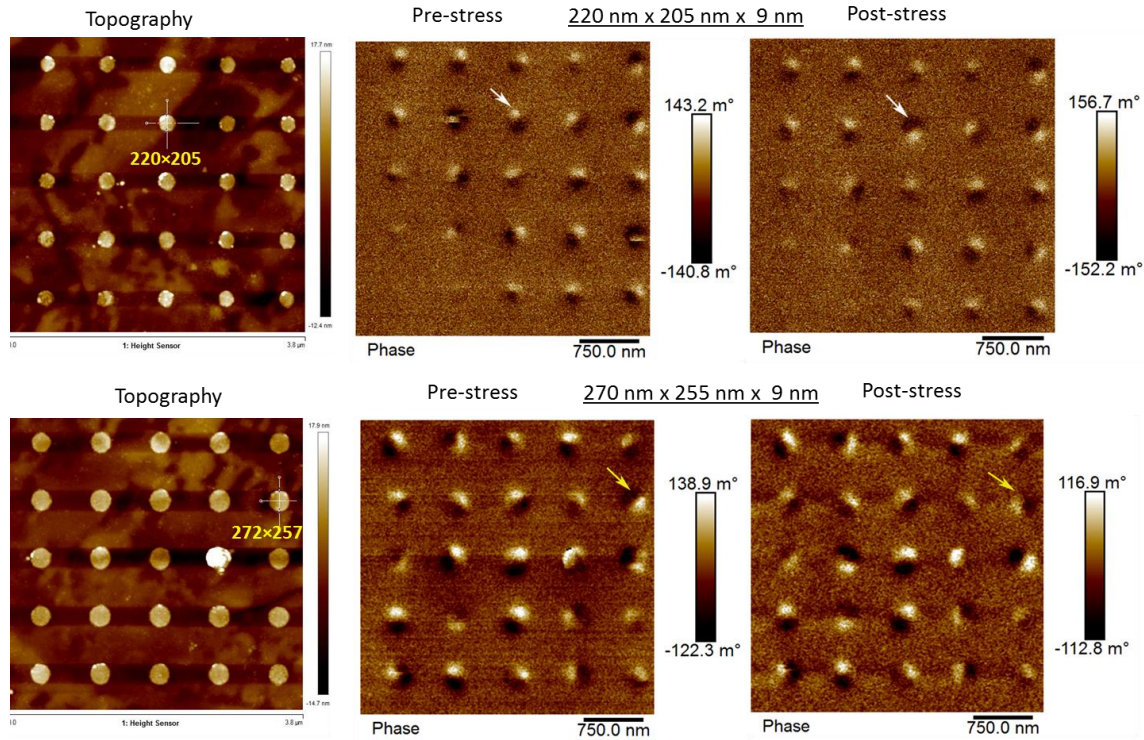
Fig. 4. 6 Pre-stress and post-stress MFM images for dimensions of 220 nm × 205 nm × 9 nm (top two subfigures) and 270 nm × 255 nm × 9 nm (bottom subfigures) on the PMN-PT substrate. One magnet switched by ~180° in one location (top subfigure) and two switched in the other (bottom subfigure) by ~150°. Actual dimensions measured for the switched magnets are 220 nm × 205 nm × 10 nm for the top and 272 nm × 257 nm × 8 nm for the bottom respectively. White and yellow arrows indicate the switched nanomagnets after the application of stress. (Lateral dimensions shown in figures are in nanometers).
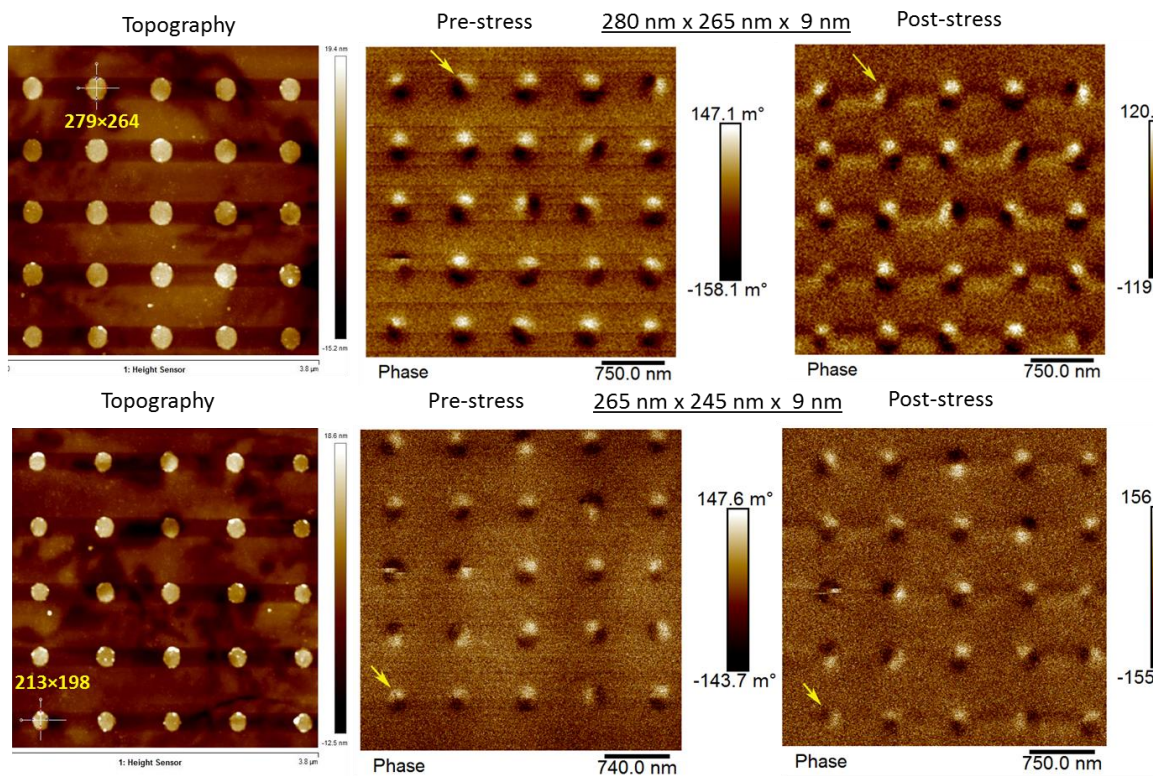
Fig. 4. 7 Pre-stress and post-stress MFM images for dimensions of 280 nm × 265 nm × 9 nm (top two subfigures) and 265 nm × 245 nm × 9 nm (bottom subfigures) on the PMN-PT substrate. Two magnet switched in one location (top subfigure) and another magnet switched in the other (bottom subfigure) by ~120°. Actual dimensions measured for the switched magnets 279 nm × 264 nm × 11 nm and 213 nm × 198 nm × 10. Yellow arrows indicate the switched nanomagnets after the application of stress. (Lateral dimensions shown in figures are in nanometers).

Table 4. 1 Switching of nanomagnets under stress: Analysis of MFM results. The nanomagnets listed in the table exhibit switching under the application of stress.

| Dimensions (in nm)	Diff. in lateral dimension (in nm)	Energy Barrier (Single domain approx.) in kT	Rotation found (in degree)
220×205×10	15	185.5	~180
272×257×11	15	230.9	~150
279×264×11	15	232.3	~120
213×198×10	15	184.07	~120
198×183×9	15	150.12	~180
198×191×9	7	70.4	~180
198×184×9	14	140.2	~180
211×203×10	8	98.3	~180
279×264×9	15	162.5	~170
264×242×9	22	234.6	~180
261×253×8	8	69.42	~120
272×257×10	20	194.9	~120

We verify our experimental results analytically for these magnets with switching behavior using single domain approximated energy profile in the plane of the magnet. Let us consider the nanomagnet of dimensions 264 nm × 242 nm × 9 nm that has been switched by ~180° and that also has the largest single domain in-plane energy barrier. Fig 4.8 shows the energy profile in the plane of the magnet under different conditions of stress. If the initial magnetization is at θ = 0° (no stress condition), then sequentially applying a uniaxial stress through axis 1, and then through axis 2, should rotate the magnetization to the other energy minimum that is at θ = 180°. We previously found that the value of uniaxial tensile stress
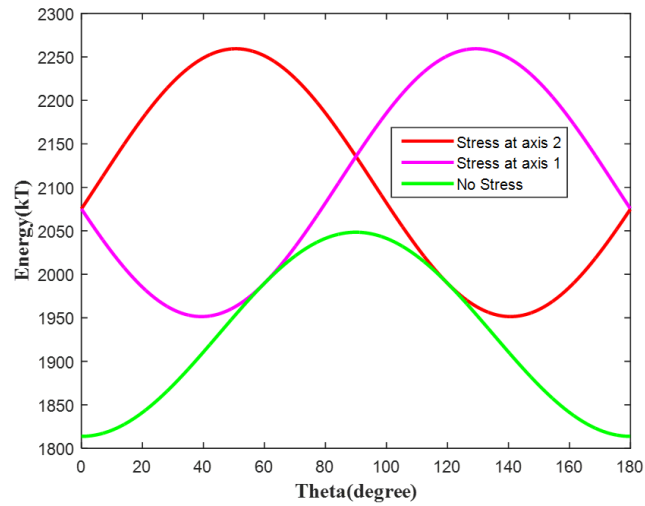
Fig. 4. 8 Energy profile in the plane of the magnet (ϕ =0) for dimension 264 nm × 242 nm × 9 nm. Stress along axis 1 should rotate the magnetization from the initial position at $\theta = 0^O$ to $\theta = \sim 40^O$. However, applying stress (125.4 MPa) along axis 2 and at the same time removing stress from axis 1 does not rotate the magnetization farther. Instead the magnetization rotates back to $\sim -40^O$. Finally, after removing stress from axis 2, the magnetization settles down to the nearest energy minimum at $\sim 0^O$ and that is the initial magnetization state. A micromagnetic simulation with 125.4 MPa of stress also shows that there is no 180° rotation of magnetization in this case (see Appendix).

generated on magnets due to a single electrode is 125.4 MPa where we ignore the fact that there is an additional compressive stress of 40.12 MPa (Poisson's ratio of Co is 0.32) generated along the axis perpendicular to the strain axis. The in-plane energy profile shown in Fig. 4.8 deals with sequential application of uniaxial stress of 125.4 MPa along two skewed axes. From the energy profile, it appears that the magnetization should not rotate from one stable state to another. However, experiments show clear evidences of 180º rotations of the magnetization. Therefore, the stress that is generated on the substrate must be much higher than 125.4 MPa either due to the presence of a pair of electrodes (instead of just one) or due to stress concentration around the magnet.

43

However, our simulation shows if there is at least ~250 MPa of stress is generated in the magnets, a complete 180° rotation of the magnetization is possible. In this case, the in-plane energy profile also shows that rotation should occur, although a FEM simulation of stress is
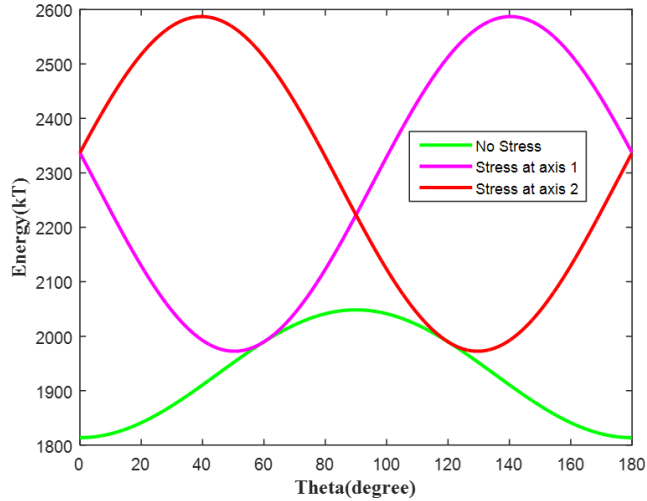
Fig. 4. 9 Energy profile on plane of the magnet (ϕ =0) for dimension 264 nm × 242 nm × 9 nm. Stress at axis 1 should rotate the magnetization by ~55° and the applying stress (~250 MPa) at axis 2 and simultaneously removing stress from 1 should rotate the magnetization by another 75° to ~130°. Final after removing stress from axis 2 magnetization settles down to the nearest energy minimum at ~180° and that is opposite to the initial magnetization state at ~0°.
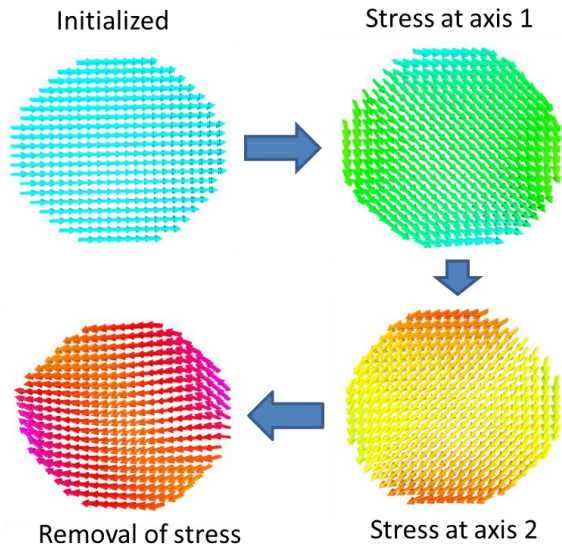
Fig. 4. 10 Magnetization dynamics at room temperature for dimension 264 nm × 242 nm × 9 nm through micromagnetic simulation with MuMax3. Results show that a rotation by 180° should happen with the uniaxial stress (~250 MPa) as indicated by the energy profile in Fig. 4.9.

44

required to capture the real scenario when voltage is applied at the pair of electrodes. We performed micromagnetic simulations for the magnetization switching of the nanomagnet under the effects of stress (~250 MPa) along two skewed axes. This was carried out using an open source simulator MuMax3 (MuMax3 (2014)). The simulation results also predict that the magnetization should rotate by 180° with stress as indicated by the energy profile in Fig. 4.9. Fig 4.10 shows the magnetization dynamics of a 264 nm × 242 nm × 9 nm nanomagnet computed with micromagnetic simulations. Therefore, at least 250 MPa of stress was generated in the magnets that switched in the experiment. The additional stress most likely come from stress concentration due to non-uniformity, defects and cracks around the magnet.

We then calculate the energy dissipation during the switching event in our experiment. We applied 300 V along the thickness of PMN-PT substrate (0.5 mm thick) which is equivalent to an electric field of 0.6 MV/m. In our experiment, CV^2 dissipation, the main contributor of energy loss is 255 nJ per sequence where capacitance is $2 \times 1000 \times 8.854 \times 10^{-12}$ x 0.4 mm × 0.4 mm / 0.5 mm = 2.83 pF (factor 2 comes from two electrode pads). In straintronic scheme, internal dissipation due to Gilbert damping is almost negligible compared to the CV^2 dissipation. Therefore, the total dissipation a switching event is 2×255 nJ = 510 nJ for applying stress in two pairs of electrodes. However, if we would have used a PMN-PT substrate of 100 nm thick, and electrode pads of 100 nm × 100 nm, the effective capacitance would be ~ 2×1000 x 8.854 × $10^{-12} \times 100$ nm × 100 nm / 100 nm = 1.7 fF. The required voltage for switching would reduce to 0.6 MV/m x 100 nm = 60 mV resulting in a CV2 loss of $2 \times 1.7\text{fF} \times (60 \text{ mV})^2$ = 12.24 aJ (2955 kT). In contrast to the dissipation in other nanomagnetic switching mechanism such as traditional

45

spin transfer torque (STT) (10^7 kT) and spin-Hall STT (10^4 kT), this straintronic version of switching nanomagnets proves to be more energy efficient.

Chapter 5. Conclusion

Computing with spintronic devices has emerged as an alternative to traditional charge-based computing over the last three decades. While computing with single spin is yet to be realized for room temperature operation, computing with single domain nanomagnet with giant spin is already making its way to commercialization. The question is whether moving an industry to a completely different technology would be viable, i.e. whether the payoff can justify the expense.. This remains to be seen. There are numerous proposals to make an energy efficient nanomagnetic switch. Unfortunately, most of them fail to lower energy dissipation compared to current CMOS. Although magnets come with the additional feature of non-volatility that enables non-Von Neuman architecture without the need for memory and logic separation, it is highly desirable that a new technology should offer some advantage in energy efficiency as well. The most standard technique of switching nanomagnets is with spin transfer torque generated from spin-polarized current either by a fixed magnetic layer or by the spin-Hall effect in non-magnetic materials. The involvement of charge current in order to produce spin current often leads to high energy dissipation. Therefore, the switching event has to occur with a voltage dropped over a very large resistance since almost no charge current flows during the switching operation if the resistance is very large. Straintronic devices utilize this advantage to generate strain in a piezoelectric material with a voltage. With the strain transferred to the magnetostrictive nanomagnet on top, switching is accomplished with very low dissipation.

In summary, we have researched various areas of the newly emerging field of "straintronics" – computing and signal processing employing strain switched nanomagnets. We have shown that mixed mode of switching (STT+SAW) can be more energy-efficient than switching with STT

alone. Better on-off ratio can be achieved by introducing two pairs of electrodes instead of one pair without sacrificing any figure of merit in a magnetoelastic memory device. A complete 180º reversal of magnetization can be implemented with geometrical arrangements of two pairs of electrodes on a piezoelectric substrate around the nanomagnet. An energy-efficient non-volatile logic gate possessing all the essential characteristics of a Boolean logic gate is proposed for the first time. We have proposed and analyzed a spintronic-straintronic reconfigurable N-bit comparator (which uses spin properties for device functionality and strain to switch the device) and showed that it is remarkably energy-efficient, relatively error-resilient and reasonably fast at room temperature. A straintronic spin neuron has been proposed and analyzed. Finally, we demonstrate complete 180º magnetization rotation in Co nanomagnets using two pairs of electrodes generating stresses along two different axes. This particular scheme, to our knowledge, has never been demonstrated before and is a very significant advance toward realizing non-volatile memory with unprecedented energy efficiency.

Appendix

Initialized   Stress at axis 1

Removal of stress   Stress at axis 2
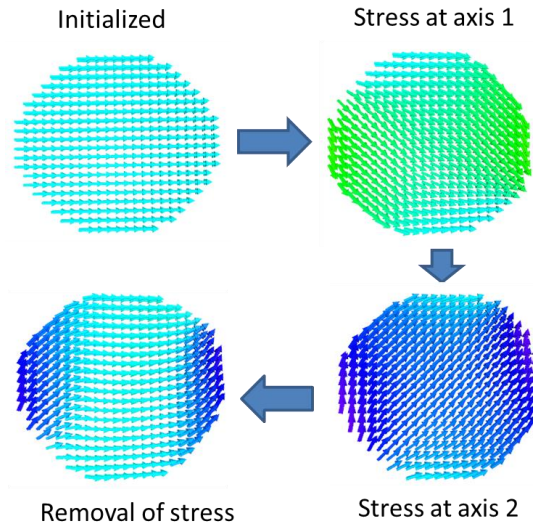
Fig. A. 1 Magnetization dynamics at room temperature for dimension 264 nm × 242 nm × 9 nm through micromagnetic simulation with MuMax3 while applying stress of 125.4 MPa sequentially along two sked axes. Results show that a rotation by 180° does not happen with the uniaxial stress (125.4 MPa) as indicated by the energy profile in Fig. 4.8.

References

Alam, M. T., Siddiq, M. J., Bernstein, G. H., Niemier, M. T., Porod, W. and Hu, X. S. (2010) "On-chip clocking for nanomagnet logic devices," *IEEE Transactions on Nanotechnology*, 9(3), pp. 348–351.

Atulasimha, J. and Bandyopadhyay, S. (2010) "Bennett clocking of nanomagnetic logic using multiferroic single-domain nanomagnets," *Applied Physics Letters*, 97, p. 173105.

Bandyopadhyay, S. and Cahay, M. (2009) "Electron spin for classical information processing: a brief survey of spin-based logic devices, gates and circuits.," *Nanotechnology*, 20(41), p. 412001.

Behin-Aein, B., Datta, D., Salahuddin, S. and Datta, S. (2010) "Proposal for an all-spin logic device with built-in memory.," *Nature Nanotechnology*, 5(4), pp. 266–70.

Biswas, A. K., Atulasimha, J. and Bandyopadhyay, S. (2014) "An error-resilient non-volatile magneto-elastic universal logic gate with ultralow energy-delay product.," *Scientific Reports*. 4, p. 7553.

Biswas, A. K., Bandyopadhyay, S. and Atulasimha, J. (2014a) "Complete magnetization reversal in a magnetostrictive nanomagnet with voltage-generated stress: A reliable energy-efficient non-volatile magneto-elastic memory," *Applied Physics Letters*, 105(7), p. 072408.

Biswas, A. K., Bandyopadhyay, S. and Atulasimha, J. (2014b) "Energy-efficient magnetoelastic non-volatile memory," *Applied Physics Letters*, 104, p. 232403.

Biswas, A. K., Bandyopadhyay, S. and Atulasimha, J. (2013) "Acoustically assisted spin-transfer-torque switching of nanomagnets: An energy-efficient hybrid writing scheme for non-volatile memory," *Applied Physics Letters*, 103(23), p. 232401.

Biswas, A. K., Atulasimha, J. and Bandyopadhyay, S. (2015) "Energy-efficient hybrid spintronic-straintronic reconfigurable bit comparator, " *Under Review*

Biswas, A. K., Atulasimha, J. and Bandyopadhyay, S. (2015a) "Straintronic spin neuron", *Under Review*

Bozorth, R. M. *Ferromagnetism*. 968 (Wiley, 1993)

Brown, W. F. (1963) "Thermal Fluctuations of a Single-Domain Particle," *Journal of Applied Physics*, 34(4), p. 1319.

Cao, H., Schmidt, V. H., Zhang, R., Cao, W., and Luo, H. (2004), Elastic, piezoelectric, and dielectric properties of 0.58Pb(Mg$_{1/3}$Nb$_{2/3}$)O$_3$-0.42PbTiO$_3$ (PMN-PT) single crystal, J. Appl. Phys. 96, 549.

Cowburn, R. P., Koltsov, D. K., Adeyeye, A. O., Welland, M. E. and Tricker, D. M. (1999) "Single-Domain Circular Nanomagnets," *Physical Review Letters*, 83(5), pp. 1042–1045.

Cowburn, R. P. and Welland, M. E. (2000) "Room Temperature Magnetic Quantum Cellular Automata," *Science*, 287(5457), pp. 1466–1468.

Cui, J., Hockel, J. L., Nordeen, P. K., Pisani, D. M., Liang, C., Carman, G. P. and Lynch, C. S. (2013) "A method to control magnetism in individual strain-mediated magnetoelectric islands," *Applied Physics Letters*, 103(23), p. 232905.

Davis, J. in *Nickel, cobalt, and their alloys*. 345 (ASM International, 2000).

Fukami, S., Suzuki, T., Nagahara, K., Ohshima, N., Ozaki, Y., Saito, S., Nebashi, R., Sakimura, N., Honjo, H., Mori, K., Igarashi, C., Miura, S., Ishiwata, N. and Sugibayashi, T. (2009) "Low-current perpendicular domain wall motion cell for scalable high-speed MRAM," Symposium on VLSI Technology, Digest of Technical Papers, pp. 230–231.

Giordano, S., Dusch, Y., Tiercelin, N., Pernod, P. and Preobrazhensky, V. (2012) "Combined nanomechanical and nanomagnetic analysis of magnetoelectric memories," *Physical Review B*, 85(15), p. 155321.

Khasanvis, S., Li, M., Rahman, M., Salehi Fashami, M., Biswas, A. K., Atulasimha, J., Bandyopadhyay, S. and Moritz, C. A.. (2015) "Self-similar Magneto-electric Nanocircuit Technology for Probabilistic Inference Engines", under review.

Long, J. Iron cobalt boride and iron zirconium silicide-based nanocomposite soft magnetic alloys and application. *ProQuest Diss. Theses; Thesis (Ph.D.)--Carnegie Mellon Univ.* (2008)

Moore, G. (1965) "Cramming more components onto integrated circuits," *Electronics*, 38(8), pp. 114–117.

MuMax3 (2014) "The design and verification of mumax3", AIP Advances 4, 107133 .

Ney, A., Pampuch, C., Koch, R. and Ploog, K. H. (2003) Programmable computing with a single magnetoresistive element. Nature 425, 485–487

Roy, K., Bandyopadhyay, S. and Atulasimha, J. (2011) "Hybrid spintronics and straintronics: A magnetic technology for ultra low energy computing and signal processing," *Applied Physics Letters*, 99(6), p. 063108.

Roy, K., Bandyopadhyay, S. and Atulasimha, J. (2012) "Energy dissipation and switching delay in stress-induced switching of multiferroic nanomagnets in the presence of thermal fluctuations," *Journal of Applied Physics*, 112(2), p. 023914.

Roy, K., Bandyopadhyay, S. and Atulasimha, J. (2013) "Binary switching in a 'symmetric' potential landscape.," *Scientific Reports*, 3, p. 3038.

Salahuddin, S. and Datta, S. (2007) "Interacting systems for self-correcting low power switching," *Applied Physics Letters*, 90(9), p. 093503.

Salehi Fashami, M., Atulasimha, J. and Bandyopadhyay, S. (2012) "Magnetization dynamics, throughput and energy dissipation in a universal multiferroic nanomagnetic logic gate with fan-in and fan-out.," *Nanotechnology*, 23(10), p. 105201.

Salehi Fashami, M., Roy, K., Atulasimha, J. and Bandyopadhyay, S. (2011) "Magnetization dynamics, Bennett clocking and associated energy dissipation in multiferroic logic.," *Nanotechnology*, 22(15), p. 155201.

Salis, G., Wang, R., Jiang, X., Shelby, R. M., Parkin, S. S. P., Bank, S. R. and Harris, J. S. (2005) "Temperature independence of the spin-injection efficiency of a MgO-based tunnel spin injector," *Applied Physics Letters*, 87(26), p. 262503.

Slobodnik, A., Conway, E. and Delmonico, R. (1973) *Microwave Acoustic Handbook*, *AFCRL-TR-73-0597*, p. 402.

Slonczewski, J. (1996) "Current-driven excitation of magnetic multilayers," *Journal of Magnetism and Magnetic Materials*, 159(1-2), pp. L1- L7.

Thevenard, L., Duquesne, J.-Y., Peronne, E., von Bardeleben, H., Jaffres, H., Ruttala, S., George, J.-M., Lemaître, A. and Gourdon, C. (2013) "Irreversible magnetization switching using surface acoustic waves," *Physical Review B*, 87(14), p. 144402.

Tiercelin, N., Dusch, Y., Klimov, A., Giordano, S., Preobrazhensky, V. and Pernod, P. (2011) "Room temperature magnetoelectric memory cell using stress-mediated magnetoelastic switching in nanostructured multilayers," *Applied Physics Letters*, 99(19), p. 192507.

Wang, K. L., Alzate, J. G. and Khalili Amiri, P. (2013) "Low-power non-volatile spintronic memory: STT-RAM and beyond," *Journal of Physics D: Applied Physics*, 46(7), p. 074003.

Yamanouchi, M., Chiba, D., Matsukura, F. and Ohno, H. (2004) "Current-induced domain-wall switching in a ferromagnetic semiconductor structure.," *Nature*, 428(6982), pp. 539–42.

Zhirnov, V. V., Cavin, R. K., Hutchby, J. A. and Bourianoff, G. I. (2003) "Limits to binary logic switch scaling-a gedanken model," *Proceedings of the IEEE*, 9(11), pp. 1934–1939.

VITA

PERSONAL INFORMATION

Name: Ayan Kumar Biswas

Date of Birth: October 02, 1988

Place of Birth: Bangladesh

Citizenship: Bangladeshi

EDUCATION

Ph.D., Virginia Commonwealth University, Richmond, VA
Electrical & Computer Engineering, May 2016
Thesis Advisor: Prof. Supriyo Bandyopadhyay

B.Sc., Bangladesh University of Engineering and Technology, Dhaka, Bangladesh
Electrical and Electronic Engineering, February 2011

WORK/RESEARCH EXPERIENCE

Graduate Research Assistant, Quantum Device Laboratory, January 2013 to present
Department of Electrical and Computer Engineering, Virginia Commonwealth University (VCU)

Graduate Research Assistant, Sensory Intelligent Laboratory, August 2012 - January 2013
Department of Electrical and Computer Engineering, Virginia Commonwealth University (VCU)

Optimization Junior Engineer, Radio Access Network Division, April 2011 to June 2012
Banglalink Digital Communications Limited, (DBA Banglalink), Bangladesh

Research Activities
- **Spintronics-straintronics paradigm for nanomagnetic memory and logic** (current)
    - Hybrid straintronic-spintronic memory
    - Nanomagnetic Boolean and non-Boolean logic implementation with strain
- **Nanoscale magnetization dynamics** (current)
    - Stress induced magnetization dynamics
    - Stochastic magnetization dynamics
    - Spin transfer torque induced magnetization dynamics
    - Magnetization dynamics in other magnetic nanostructures involving spin orbit torques
- **Experiments on straintronic memory devices** (current)
    - Fabrication and characterization of a Co based straintronic memory device

- **Sensor based design**
    - Fiber optic sensor-based mosquito trap design
- **Gene-data classi_cation**
    - Classi_cation of yeast microarray gene expressions using digital signal processing
- **Multi-valued logic**
    - Realization and synthesis of Ternary and quaternary circuits using quantum gates

Research Interest
- **Spintronics and nanomagnetism**
- **Magnetic materials and multiferroics**
- **Magnetization dynamics**
- **Spin Hall state**

Publications: Peer-Reviewed Journal Papers
- **A. K. Biswas**, J. Atulasimha, S. Bandyopadhyay, Energy-efficient hybrid straintronic-spintronic re-configurable bit comparator, *Under Review*, 2015
- M. S. Fashami, N. D'Souza, **A. K. Biswas**, S. Bandyopadhyay and J. Atulasimha, Topical Review: Hybrid straintronics-spintronics, *Under Review*, 2015
- S. Khasanvis, M. Li, M. Rahman, **A. K. Biswas**, M. S. Fashami, J.Atulasimha, S. Bandyopadhyay, and C. A. Moritz, Architecting for Causal Intelligence at Nanoscale, *In press with Computer, IEEE Computer Society*, 2015
- S. Khasanvis, M. Li, M. Rahman, M. S. Fashami, **A. K. Biswas**, J.Atulasimha, S. Bandyopadhyay, and C. A. Moritz, Self-similar Magneto-electric Nanocircuit Technology for Probabilistic Inference Engines, *In Press with IEEE Trans. Nanotechl.*, 2015
- **A. K. Biswas**, J. Atulasimha, S. Bandyopadhyay, Spintronic spin neuron, *Nanotechnology*, 26, 285201,2015
- **A. K. Biswas**, J. Atulasimha, S. Bandyopadhyay, An error-resilient non-volatile magneto-elastic universal logic gate with ultralow energy-delay product, *Sci. Rep.* 4, 7553, 2014
- **A. K. Biswas**, S. Bandyopadhyay, J. Atulasimha, Complete magnetization reversal in a magnetostric-tive nanomagnet with voltage-generated stress: A reliable energy-efficient non-volatile magneto-elastic memory, *Appl. Phys. Lett.*, 105, 072408, 2014
- **A. K. Biswas**, S. Bandyopadhyay, J. Atulasimha, Energy-efficient magnetoelastic non-volatile memory, *Appl. Phys. Lett.*, 104, 232403, 2014
- **A. K. Biswas**, S. Bandyopadhyay, J. Atulasimha, Acoustically assisted spin-transfer-torque switching of nanomagnets: An energy-efficient hybrid writing scheme for non-volatile memory, *Appl. Phys. Lett.* 103, 232401, 2013
- **A. K. Biswas**, N. Siddique, B. B. Tian, E. Wong, K.Caillouet, Y. Motai, Design of a Fiber-optic Sensing Mosquito Trap, *IEEE Sensors Journal*, vol-13, pp- (4423 - 4431), 2013.

Publications: Conference Proceedings
- H. Ahmad, **A. K. Biswas**, J. Atulasimha, S. Bandyopadhyay, Straintronics: Strain-switched mul-tiferroic nanomagnets for extremely low energy logic/memory, IEEE Nanotechnology Materials and Devices Conference (NMDC), 2015
- S. Khasanvis, M. Li, M. Rahman, M. S. Fashami, **A. K. Biswas**, J.Atulasimha, S. Bandyopadhyay, and C. A. Moritz, Physically equivalent magneto-electric nanoarchitecture for probabilistic reasoning, *Accepted in 11th IEEE/ACM International Symposium on Nanoscale Architectures*, 2015

- **A.K. Biswas**, M.M. Al-Rashid, J. Atulasimha, S. Bandyopadhyay, Magneto-elastic arti_cial neurons with extremely low energy dissipation, *Bulletin of the American Physical Society* 60, 2015
- **A. K. Biswas**, S. Chouwdhury, M.M.M. Khan, M. Hasan, A. I. Khan, Some Basic Ternary Operations Using Toffoli Gates Along with the Cost of Implementation, *41st IEEE International Symposium on Multiple-Valued Logic (ISMVL)*, pp(142-146), 34, 2011
- M.M.M. Khan, **A. K. Biswas**, S. Chowdhury, M. Hasan, A. I. Khan, Synthesis of GF(3) Based Reversible/Quantum Logic Circuits without Garbage Output, *41st IEEE International Symposium on Multiple-Valued Logic (ISMVL)*, pp(98-102), 73, 2009
- M.M.M Khan, **A. K. Biswas**, S. Chowdhury, M. Tanzid, K.M. Mohsin, M. Hasan, A. I. Khan, Quantum realization of some quaternary circuits, *IEEE Region 10 Conference TENCON* pp(1-5), 4766486, 2008

Talks
- *Low Power Straintronics: Nanomagnetic computing devices robust to thermal noise*, NRI e-workshop, on behalf of Prof. Supriyo Bandyopadhyay, August, 2015
- **Invited talk** on *Hybrid Spintronics and Straintronics: An ultra-energy-efficient approach for nano-magnetic logic and memory*, Energy Frontier Research Center Seminar, SHINES center, University of California, Riverside (UCR), 2015
- *Hybrid Spintronics and Straintronics: An ultra-energy-efficient approach for nanomagnetic logic*, Under Hybrid Spintronics and Straintronics: Annual Review, VCU NEB2020 NRI-NSF Virtual Visit, June, 2015
- *Hybrid Straintronic Memory Devices towards low power computing*, Under Hybrid Spintronics and Straintronics: Annual Review, VCU NEB2020 NRI-NSF Virtual Visit, May, 2014
- *Acoustic Wave Switching of Nanomagnets*, Under Hybrid Spintronics and Straintronics: Annual Review, VCU NEB2020 NRI-NSF Virtual Visit, June, 2013

Book Chapter
- Hybrid Spintronics-Strainronics, **A. K. Biswas**, S. Bandyopadhyay, N. D'Souza, and J. Atulasimha. (Under Preparation with Wiley).

Patent
- Magneto-elastic non-volatile multiferroic logic and memory with ultralow energy dissipation, S. Bandyopadhyay, J. Atulasimha, **A. K. Biswas**. (Pending).

News Highlight
- **Phys.org (featured)** : `Straintronic spin neuron' may greatly improve neural computing, 2015.
- **Phys.org** : Non-volatile memory improves energy efficiency by two orders of magnitude, 2014.

Organizations
- *Member*, American Physical Society, September 2014 to Present
- *Member*, Phi Kappa Phi, November 2013 to Present
- *Student Member*, IEEE, November 2012 to Present
- *General Secretary*, Cricket Club at VCU, November 2014 to present

Technical Service
- *Reviewer,* (Journal Manuscript), IEEE Transaction of Electron Device, 2016.

Scholarships and Awards

- Outstanding Research Award 2015, Department of Electrical & Computer Engineering (VCU)
- Special Media Coverage for Journal Paper 2015, Department of Electrical & Computer Engineering (VCU)
- Outstanding Graduate Research Award 2014-2015, Engineering Students Association (VCU)
- School of Engineering 2015-2016 Phi Kappa Phi Scholarship (VCU chapter)
- GMAG student travel award - 2015 (APS March Meeting)
- Phi Kappa Phi Membership Certificate for being among top 10% students in VCU - 2013
- Merit List Scholarships in final semester of B.Sc Engineering studies for obtaining GPA 4.00 - 2011
- Dean's List Scholarships in second and final year of B.Sc Engineering studies for maintaining CGPA on or above 3.75 - 2007 & 2009
- 1st grade government scholarships with full tuition, text-book waiver for excelling in Higher Secondary Certificate Examination throughout the undergraduate studies - 2006 to 2010
- General Manager's Gold Medal from Sonali Bank, Bangladesh for outdoing in Higher Secondary Certificate - 2005
- General Manager's Gold Medal from Sonali Bank, Bangladesh for outstanding result in Secondary School Certificate - 2003
- Primary and Junior School Examination scholarship throughout secondary school studies - 1998 & 2000